A model predictive vertical motion control of a passenger ship

Kucukdemiral, Ibrahim Beklan; Cakici, Ferdi; Yazici, Hakan

Published in:
Ocean Engineering

DOI:
10.1016/j.oceaneng.2019.06.005

Publication date:
2019

Document Version
Author accepted manuscript

A Model Predictive Vertical Motion Control of a Passenger Ship

Ibrahim Beklan Kucukdemiral[1]

Glasgow Caledonian University, School of Computing, Engineering and Built Environment, Department of Applied Science, Glasgow, UK

Ferdi Cakici[2]

Yildiz Technical University, Department of Naval Architecture and Marine Engineering, Istanbul, Turkey

Hakan Yazici[3,]

Yildiz Technical University, Department of Mechanical Engineering, Istanbul, Turkey

Abstract

In this study, the design problem of a Model Predictive Controller (MPC) for attenuation of vertical motions of a passenger ship which is subject to irregular wave excitations is investigated. The proposed design considers actuator amplitude and rate saturation phenomenon. The motion control system of the ship utilises a pair of active stabilizing fins mounted to the head and tail. First, irregular long crested head waves are implemented by a well-established randomization theory in order to find heave force and pitch moment at $F_n = 0.40$ and $F_n = 0.50$ in the time domain. Then, a two-degree-of-freedom mathematical model, in which pitch and heave motions are coupled with the approximation of convolution integrals is solved to obtain the uncontrolled motions and accelerations of the ship. Finally, considering the physical amplitude and rate limitations of the active fin mechanism, an MPC design is proposed to obtain a practically applicable state-feedback control law for attenuating vertical motion of a passenger ship. The performance of the MPC is also compared with an elipsoid based $\mathcal{H}_\infty$ controller. An extensive amount of simulation studies are presented at the end to illustrate the effectiveness of the proposed approach.

Keywords: Model Predictive Control, $\mathcal{H}_\infty$ Control, Magnitude and Rate Saturated Actuators, Vertical Motion of Ship, Irregular Sea Waves, Seasickness

2010 MSC: 00-01, 99-00

*Corresponding author
Email address: hyazici@yildiz.edu.tr (Hakan Yazici)
[1]Glasgow G4 0BA
[2]34349 Yildiz-Istanbul
[3]34349 Yildiz-Istanbul

1. Introduction

Seakeeping ability of a ship is strongly associated with the improvements of undesired motions in rough seas. Seasickness level of passengers on board should be reduced sufficiently for passenger comfort and crew operability. The first experimental studies that reveal the influence of ship vertical accelerations on the human body were conducted by O'Hanlon and McCauley in 1974 [1]. This experimental work was carried out with a large group of voluntary male students. Subjects were undergone different amplitude of acceleration at different oscillation frequencies in order to observe vomiting tolerance. According to the results of this work, number of graphs were plotted describing the seasickness regions by means of the frequency and amplitude of the oscillation. Additionally, it is understood that the most dangerous frequency to the human body is in the vicinity of 1 rad/s and seasickness incident is proportional to the exposure time. Since most wave frequencies at sea are observed in the vicinity of 1 rad/s, reducing the pitch motion of the ship by a control system is required for safer operations in a seaway.

The techniques used to reduce the pitch motion of ships have been primarily passive. However, using passive methods has significantly increased the resistance of the ship [2], [3], [4]. Hence, it is understood that when the forward speed of the ship is higher than $10 - 15$ knots, active actuators such as fins yielded more effective solutions [5],[6].

It is well known that controller design plays a significant role in ship motion control. Therefore, a large variety of control approaches for reducing the vertical motions of ships have been presented in the literature. A proportional, integral, derivative (PID) based controller with the aim of reducing pitch and heave acceleration for a high-speed ferry form using flap and T-foil is proposed in [7]. An experimental campaign was carried out in [8] to demonstrate the effectiveness of active control to damp the vertical motion of a scaled down replica of a fast ferry. In this study, vertical accelerations which are the main cause of seasickness has been reduced with a fuzzy control system based on the fuzzy model of a ship is proposed in [9]. A new model-free control approach to reduce the vertical motions induced by random waves on a high–speed ferry was also introduced at [10],[11]. In these studies, a comparison study between Proportional-Derivative (PD) and so-called i-PD (intelligent PD) was performed and the results showed that i-PD exhibited a better ability to handle the varying system parameters and operating velocity. On the other hand, Zhang *et al.* proposed a $\mathcal{H}_\infty$ output feedback control method using Ricatti equations to reduce the longitudinal motion and the sickness incidence of the wave piercing catamaran. They used instantaneous heave and pitch velocities as feedback signals [12]. [6] applied a numerical and experimental study for pitch stabilization in head waves. In this work, a short term predictor has been proposed to predict hydrodynamic forces. Then these predicted motions are used in a force estimator to forecast the ship's hydrodynamics. In a similar way, [13] studied on pitch-roll stabilization problem by active fins. However, although the proposed control strategy considers magnitude bound on the angle-of-attack, it does not consider any rate

constraint on the control signal which makes it difficult to realise on a full-sized ship having huge control fins with very large time constants. Similarly, a Linear Matrix Inequality (LMI) based robust static output feedback $\mathcal{H}_\infty$ controller design was developed in [14] to mitigate vertical acceleration of a motor yacht form. Among these aforementioned works, it is apparently seen that to the best of our knowledge, no study exists in literature utilizing the MPC strategy for reducing vertical ship motion by the use of anti-pitching. Moreover, actuator amplitude and rate saturation problems have never been jointly taken into consideration in controller design as provided in this paper. These investigations motivate us to develop a practically applicable model predictive controller for ships having actuator amplitude and fin velocity saturation. It is noted that the optimal $\mathcal{H}_\infty$ controller is also applied in this paper in order to have comparative results.

In this work, a disturbance attenuation type discrete-time MPC under different wave conditions and ship forward speeds is proposed which considers actuator amplitude and rate saturation. The popularity of MPC arises from the fact that the resulting control action respects all the system and problem information, in conjunction with interactions and constraints of the system parameters, which would be very difficult to achieve by any other controller [15]. The bounds on the rate of the actuator force (torque, thrust, etc.) have also been identified as a source of severe performance degradation or instability in control applications and might yield critical limitations on the system[16]. Different from the literature, the aim of this study is to develop a more realistic, practically implementable optimal controller which attenuates vertical motions of a passenger ship subject to irregular wave disturbances by respecting actuator constraints.

This paper is organized in a way to develop from modelling of a ship and wave disturbance to the MPC design for the active foil system having actuator amplitude and rate saturation. Therefore, Section 2 describes the mathematical model of the ship and the wave disturbance. Disturbance rejection type MPC strategy is developed in Section 3. Section 4 considers the design of a discrete-time state feedback $\mathcal{H}_\infty$ controller for systems having magnitude and rate based actuator limitations. Section 5 provides extensive simulations on the system under different sea conditions and ship speeds. Finally, Section 6 concludes the paper with some final remarks on possible research directions. The paper is further structured into subsections for better readability.

Notation. Throughout the paper, a fairly standard notation is used. The symbol $\mathbb{R}$ denotes the set of real numbers, $\mathbb{R}^{m\times n}$ stands for $m \times n$ matrices having real entries. Column vectors having n entries are represented by $\mathbb{R}^n$. The symbol $\hat{}$ is used to represent estimated signals. $\|z\|_Y^2$ stands for the quadratic term $z^T Y z$. $0_{m\times n}$ denotes a rectangular null matrix having a size $m \times n$ whereas I_n represents a square $n \times n$ identity matrix. Lower case italic letters are generally used to represent vectors whereas capital italic letters are used for matrices. An ellipsoidal set having a weighting matrix $P = P^T \succ 0$ and centred at the origin is defined as

$$\mathbf{Elp}(P) \triangleq \left\{x \,|\, x^T P x \leq 1\right\} \tag{1}$$

For matrices and vectors, $(\cdot)^T$ indicates the transpose operator. For symmetrical matrix elements, $\star$ denotes the transposed symmetric element induced by the symmetry. $\mathcal{X} \preceq (\succeq) 0$ indicates that $\mathcal{X}$ is a negative semi-definite (possitive semi-definite) matrix. $\text{diag}\{X, Y\}$ stands for the diagonal matrix having elements X and Y on its main dioganal. Finally, $\mathbf{sup}\, X$ stands for the supremum (smallest upper bound) of a set X.

2. Mathematical Model of a Passenger Ship

During the derivation of the mathematical model, Cummins' equation is used to represent the vertical ship motions of the considered passenger ship subject to irregular waves. First, the frequency domain coefficients are calculated using an in house code based on strip theory. Then, the convolution integrals used in the equation of motions are approximated by a well-known time-domain identification method. Finally, irregular head wave scenario is realized with wave-based excitation signals by the randomization theory.

2.1. Ship Model

In this study, we consider a passenger ship of $L_{WL} = 42.95$ metres waterline length, 5.3 metres in breadth, 205 tons of mass and $2011.05kN$ of displacement force. In the static condition, the location of the centre of gravity (LCG) is assumed to be the same as the centre of buoyancy (LCB) which is 18.67 metres from the transom. The mass inertia moment for pitch motion, $\mathcal{I}_5 = 23385\,\text{tonm}^2$ and the advance velocity V of the ship is assumed to be 8.2304m/s and 10.288m/s. Figure 1 shows the sketch of the ship, excited with irregular long-crested head waves, in the global coordinate axis. The direction of the ship longitudinal axis is aligned to the opposite direction of the incoming waves. So the heading angle is 2π for the head waves. Note that, in this paper, heave motion is negative from the origin downwards while pitch motion is negative when the bow of the ship goes up.

2.2. Cummins equation for coupled heave and pitch motions

Vertical motions of ship in a rough sea condition having a constant forward speed V can be modelled by using Cummins' Equation [17] as follows:

$$(\bar{M} + A^{\infty})\ddot{z}(t) + B(V)\dot{z}(t) + \int_0^t K(t-\tau)\dot{z}(\tau)d\tau + Cz(t) = F_E(t) \tag{2}$$

where, $\bar{M}$ stands for the ship mass, A^{∞} denotes the mass matrix at the infinite frequency, $B(V)$ is the constant damping matrix, C is the restoring matrix which is a function of only geometry, $z(t)$ is the oscillatory response of the ship and finally $F_E(t)$ is the transient wave force vector that can be created by a linear superposition of frequency domain results based on different wave spectra. On the other hand, $K(t)$ is the impulse response function matrix which is defined as

$$K(t) = \frac{2}{\pi}\int_0^{\infty} [B(\omega_e) - B(V)]\cos(\omega_e t)d\omega_e \tag{3}$$

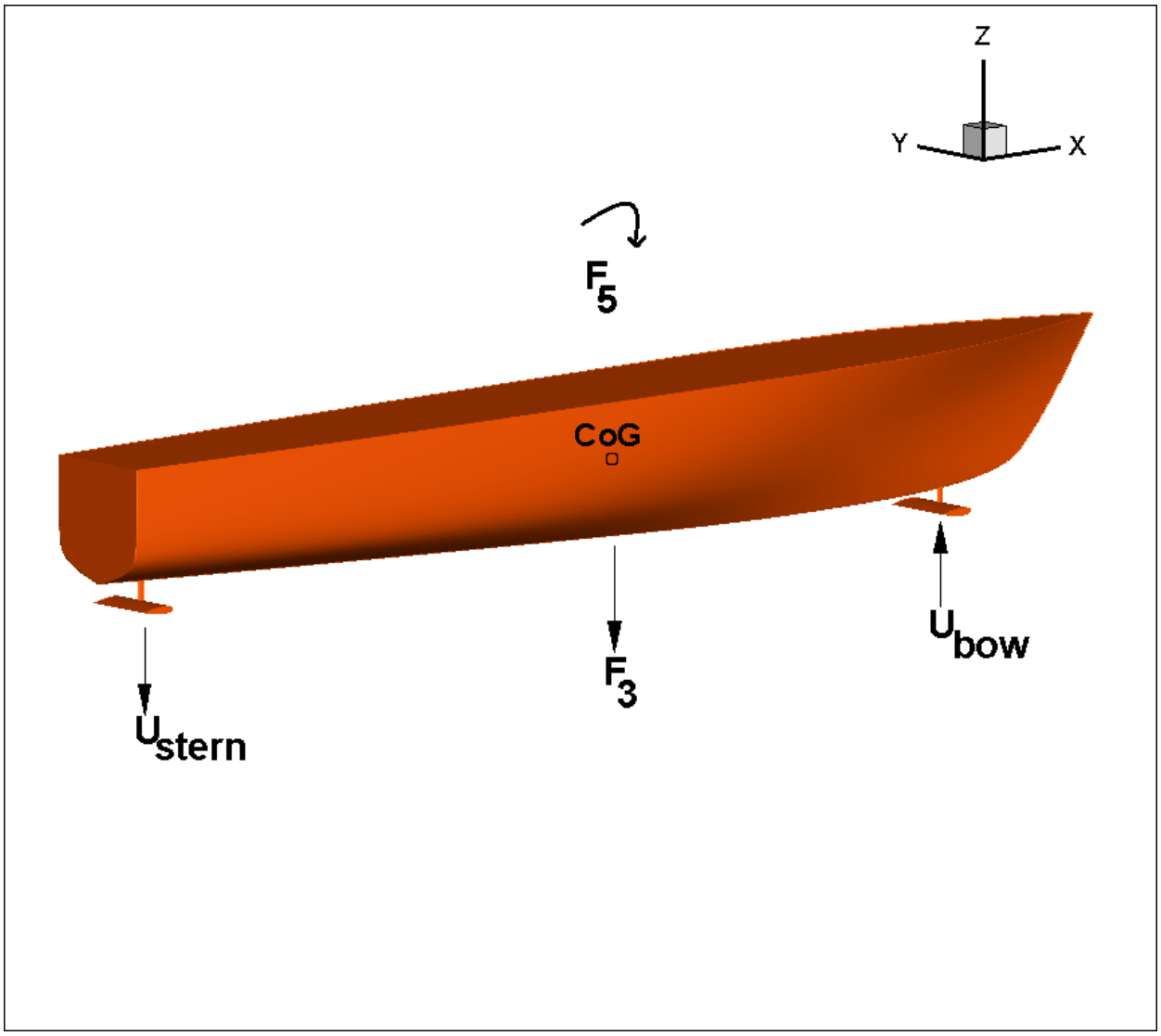

Figure 1: The sketch of a ship under head wave excitation.

Here, $B(\omega_e)$ is the damping matrix in frequency domain. ω_e denotes the encounter frequency whose value can be obtained by the equation, $\omega_e = \omega + (kV)$ for the head waves where ω denotes the wave frequency and k denotes the wave number.

Then the coupled Cummins' Equations for the vertical motion of the ship advancing with a constant speed V can be re-written as follows:

$$(\bar{M} + A_{33}^{\infty})\ddot{z}_3(t) + B_{33}(V)\dot{z}_3(t) + \int_0^t K_{33}(t-\tau)\dot{z}_3(\tau)d\tau + C_{33}z_3(t) + A_{35}^{\infty}\ddot{z}_5(t) + B_{35}(V)\dot{z}_5(t) + \int_0^t K_{35}(t-\tau)\dot{z}_5(\tau)d\tau + C_{35}z_5(t) = F_3(t) \quad (4)$$

$$(\mathcal{I}_5 + A_{55}^{\infty})\ddot{z}_5(t) + B_{55}(V)\dot{z}_5(t) + \int_0^t K_{55}(t-\tau)\dot{z}_5 d(\tau) + C_{55}z_5(t) + A_{53}^{\infty}\ddot{z}_3(t) + B_{53}(V)\dot{z}_3(t) + \int_0^t K_{53}(t-\tau)\dot{z}_3(\tau)d\tau + C_{53}z_3(t) = F_5(t) \quad (5)$$

Here, $z_3(t)$, $\dot{z}_3(t)$, $\ddot{z}_3(t)$ are the heave motion, heave velocity and heave acceleration of the ship whereas $z_5(t)$, $\dot{z}_5(t)$, $\ddot{z}_5(t)$ are the pitch motion, pitch velocity and pitch acceleration of the ship, respectively. $F_3(t)$ represents the heave force based on irregular waves whereas $F_5(t)$ represents the pitch moment based on irregular waves in time domain. Further, $\mathcal{I}_5$ is the ship inertia moment for pitch motion. A_{ij}^{∞} is the added mass coefficient at infinite frequency. $K_{ij}(t)$ is the impulse response function whereas C_{ij} is the restoring coefficient for the motion in mode i with respect to the motion in the mode j. $B_{ij}(V)$ appears in Cummins' equation if the ship has a forward speed. Note that these terms have approximated values at infinite frequency and their values are obtained using the Riemann-Lesbesque Lemma [18]. Therefore, $B_{ij}(V) = B_{ij}^{\infty}$ where $i = \{3, 5\}$ and $j = \{3, 5\}$. The value of A_{ij}^{∞} is dependent only on the ship geometry and can be obtained by the convergence value from the frequency domain graphs. Similarly, restoring values, C_{ij} are also dependent on the ship geometry and can be calculated with the geometric properties of the ship.

2.3. Calculation of Radiation Terms

$K_{ij}(t)$ is the impulse response function which can be calculated as

$$K_{ij}(t) = \frac{2}{\pi}\int_0^{\infty}[B_{ij}(\omega_e) - B_{ij}^{\infty}]\cos(\omega_e t)d\omega_e \quad i, j = \{3, 5\} \quad (6)$$

where the damping coefficient, $B_{ij}(\omega_e)$ is obtained by using strip theory implemented in an in-house code as shown in Figure 2. Note that the definite integrals for impulse response functions defined in (6) are calculated in the encounter frequency range and their variations are demonstrated in Figure 3. In the present study, the definite integrals for impulse response functions defined above are calculated for a particular frequency range, $0.6 - 4$rad/s. The frequencies lower than 0.6 rad/s and higher than 4 rad/s are ignored because the ship has almost zero response beyond this frequency range. Please note that the impulse response functions are chosen identical for the ship advance speeds which are 8.2304m/s and 10.288m/s since the encounter frequency range is set sufficiently large. Hence,

$$K_{ij}(t) \cong \frac{2}{\pi}\int_{0.6}^{4}[B_{ij}(\omega_e) - B_{ij}^{\infty}]\cos(\omega_e t)d\omega_e \quad (7)$$

However, it is still a very time-consuming process to calculate (4) and (5) due to the existence of the

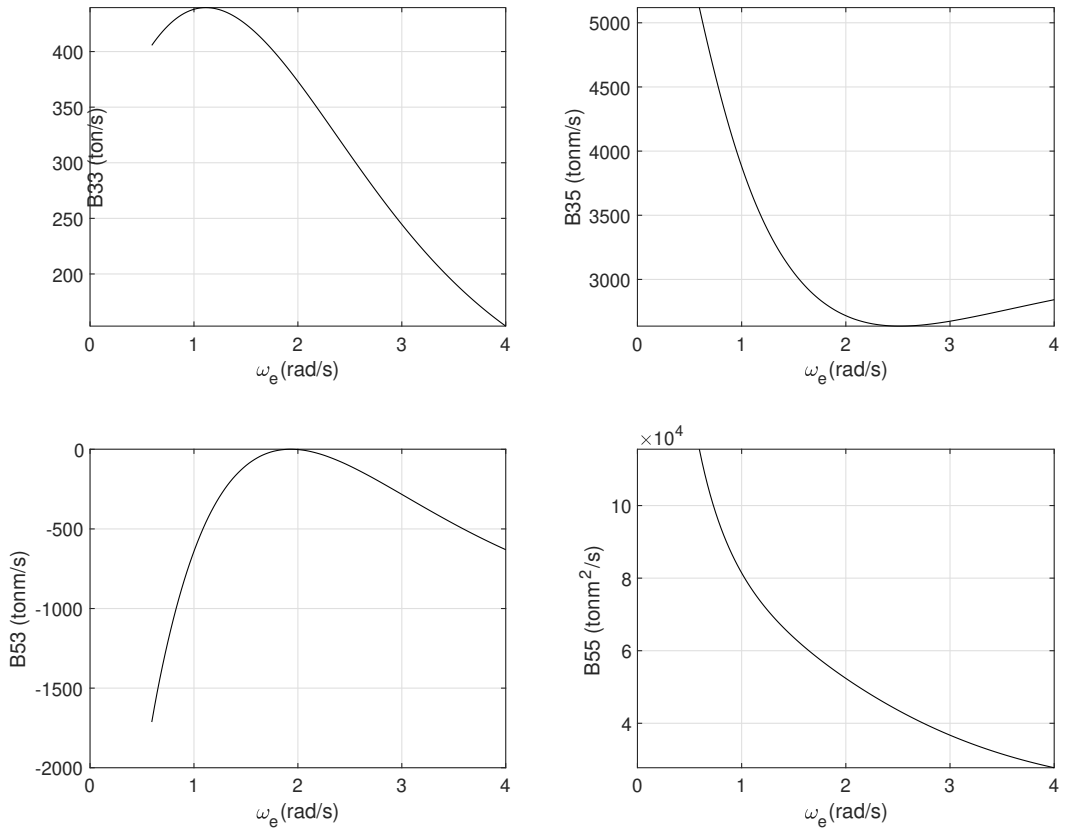

Figure 2: Damping-w_e relations.

following terms which include convolutions:

$$\eta_1(t) \triangleq \int_0^t K_{33}(t-\tau)\dot{z}_3 d(\tau) + \int_0^t K_{35}(t-\tau)\dot{z}_5 d(\tau)$$
$$\eta_2(t) \triangleq \int_0^t K_{53}(t-\tau)\dot{z}_3 d(\tau) + \int_0^t K_{55}(t-\tau)\dot{z}_5 d(\tau) \tag{8}$$

Note that the direct implementations of these convolution integrals, as underlined above, are computationally expensive, especially for the control applications such as model predictive control where a huge amount of information is being processed in real-time. Therefore, in this study, these convolution terms are approximated with suitable transfer functions. Following [19], in this note, filters that are obtained by using Prony's method are utilised to approximate each impulse function. Prony's method is a technique for modelling discrete data as a linear combination of exponentials. Although it cannot be classified as a spectral estimation technique, it has a close relationship with the least squares based system identification algorithms [20]. Using the Prony's method along with system identification techniques, one can obtain the

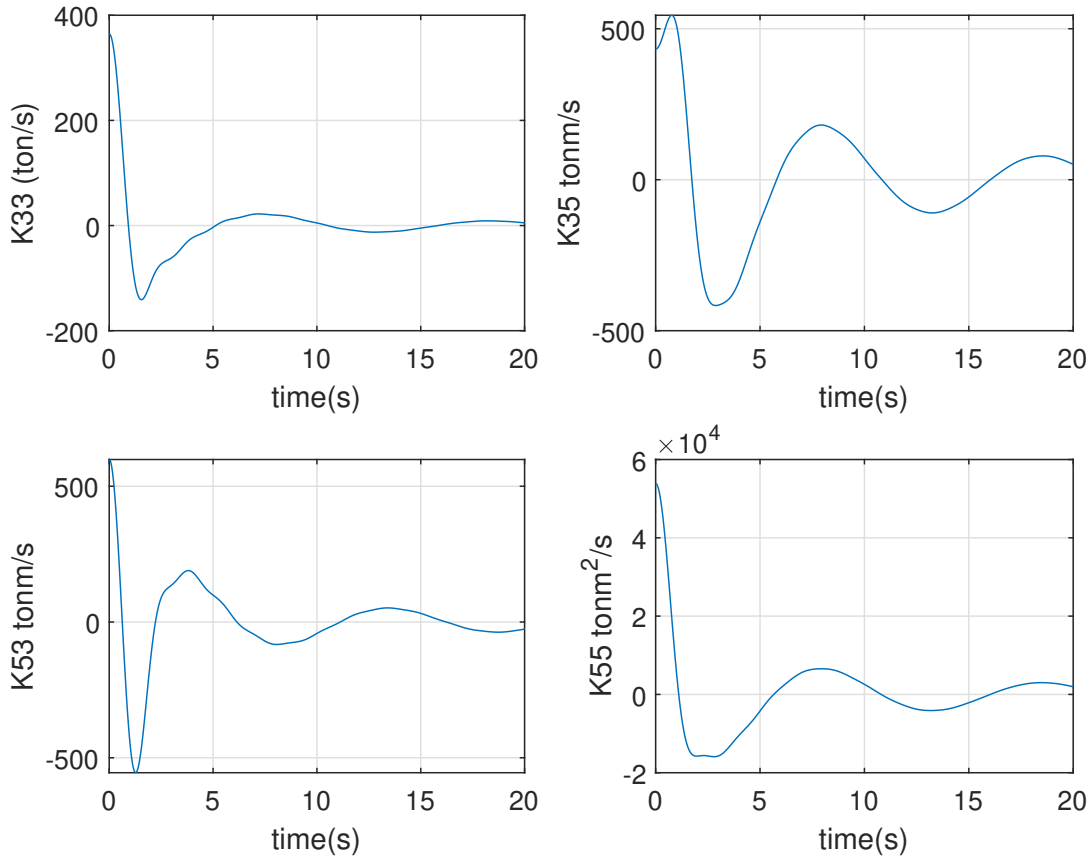

Figure 3: Impulse Response Functions.

approximated transfer functions for K_{33}, K_{35}, K_{53} and K_{55} as follows:

$$K_{33}(s) \cong \frac{364.51s^5 - 1810.8s^4 + 3598.9s^3 - 3576.7s^2 + 1777.6s - 353.42}{s^6 - 5.96s^5 + 14.84s^4 - 19.68s^3 + 14.68s^2 - 5.84s + 0.96} \tag{9}$$

$$K_{35}(s) \cong \frac{432.47s^5 - 2156.3s^4 + 4301.1s^3 - 4290.4s^2 + 2140.2s - 427.13}{s^6 - 5.98s^5 + 14.93s^4 - 19.86s^3 + 14.86s^2 - 5.93s + 0.98} \tag{10}$$

$$K_{53}(s) \cong \frac{598.49s^5 - 2981.2s^4 + 5940.6s^3 - 5919.6s^2 + 2949.6s - 587.96}{s^6 - 5.98s^5 + 14.90s^4 - 19.81s^3 + 14.81s^2 - 5.91s + 0.98} \tag{11}$$

$$K_{55}(s) \cong \frac{53875.3s^5 - 267779.8s^4 + 532457.01s^3 - 529444.10s^2 + 263259.89s - 52368.2}{s^6 - 5.97s^5 + 14.85s^4 - 19.71s^3 + 14.71s^2 - 5.85s + 0.97} \tag{12}$$

As it can be seen from Figure 4, the Prony approximations represent the retardation functions with very high accuracy, particularly at the first instants of the impulse response. In this work, following a few trials, we decided to use a 6^{th} order approximation. However, more accurate results could be obtained by using higher order filters albeit at a high computational cost.

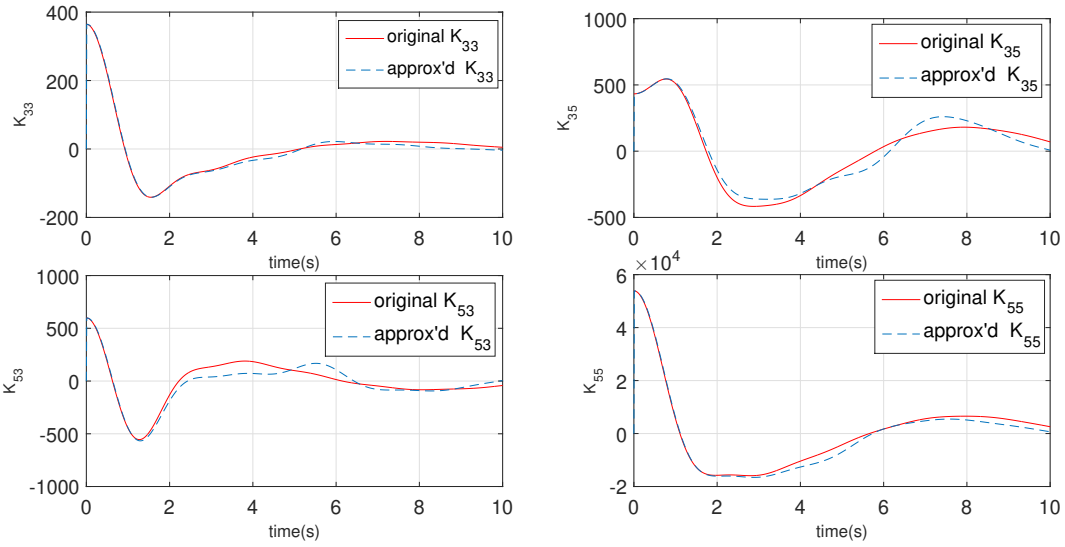

Figure 4: Representation of Impulse Response Functions with LS Method.

2.4. Prediction of Excitation Terms

It is very common to define a wave spectrum in order to represent the behaviour of ocean waves. If there are sufficient data from wave ride bouys, the wave spectrum can be obtained by spectral estimation techniques [5]. If these measurements are not available directly, then the idealized wave spectrum formulae can be used. In this paper, Pierson-Moskowitz spectrum, one of the most famous idealised spectrum to define the distribution of energy with frequency within the ocean, is applied.

Pierson-Moskowitz spectrum [21] can expressed as

$$S_\zeta(\omega) = A\omega^{-5}e^{-\frac{B}{\omega^4}} \tag{13}$$

where the frequency domain is used to represent excitation terms. Here, ω stands for the frequency in radians per second whereas $S_\zeta(\omega)$ denotes the encounter wave energy spectrum. In line with the physical parameters listed in Table 2, one can obtain the constants A and B as follows:

$$A = 0.0081 \times g^2 \tag{14}$$

$$B = \frac{0.032g^2}{H_s^2} \tag{15}$$

where H_s denotes the characteristic wave height and g denotes the acceleration of gravity. In this study, three different significant wave height conditions (0.70, 0.88 and 1.0 metres) were considered during the simulation of irregular waves. For the excitation term predictions, the linear superposition principle which was proposed in [22] is used. Hence,

$$S_{\mathrm{HF/PM}}(\omega_e) = S_\zeta(\omega_e) \times |TF_{\mathrm{HF/PM}}(\omega_e)|^2 \tag{16}$$

where, $S_\zeta(\omega_e)$ can be calculated as

$$S_\zeta(\omega_e) = \frac{S_\zeta(\omega)}{1 + \frac{2V\omega}{g}} \tag{17}$$

For example, wave encounter energy spectrum $S_\zeta(\omega_e)$, is plotted in Figure 5 for $H_s = 0.88$. In (16), $TF_{\mathrm{HF/PM}}(\omega_e)$ denotes the heave force or pitch moment in regular head waves while the ship has a forward speed $V = 10.288$m/s and they are given in Figure 6. Please note that different ship advance speeds refer to different wave excitations under the same wave conditions. On the other hand, $S_{\mathrm{HF/PM}}(\omega_e)$ stands for the heave force or pitch moment response spectrum for the investigated wave. According to linear random

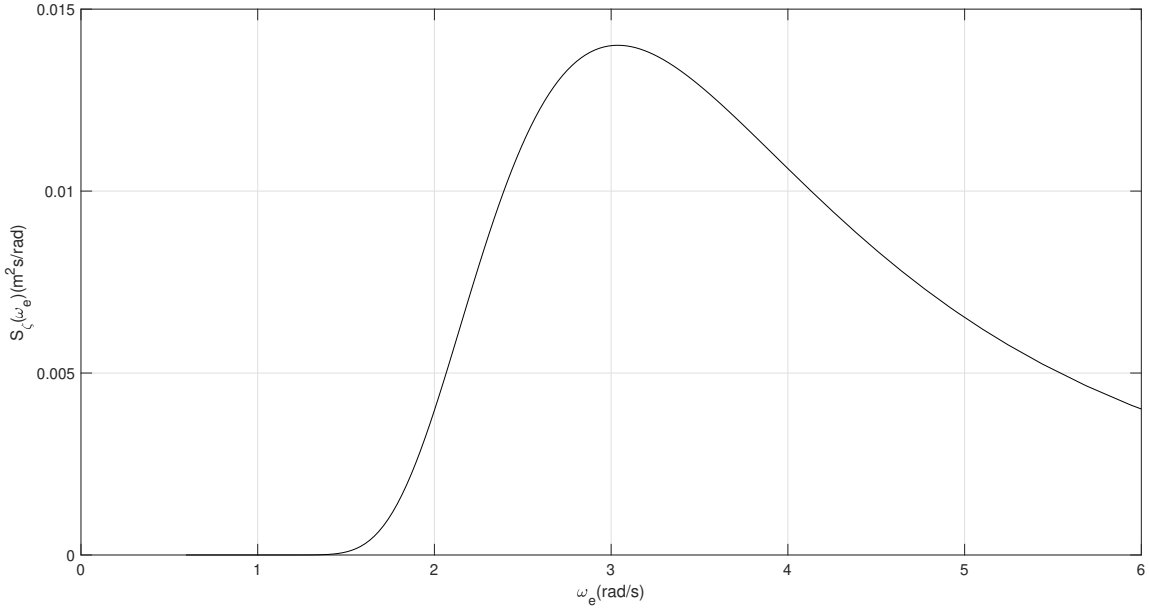

Figure 5: Wave encounter energy spectrum $S_\zeta(\omega_e)$ for $H_s = 0.88$ m.

wave theory, unidirectional and long-crested waves can be expressed by the sum of finite regular waves. Therefore, instantaneous wave amplitude can be stated as

$$\zeta(x,t) = \sum_{i=1}^{N_i} A_i \sin(\theta_i(t)) \tag{18}$$

where $\zeta(x,t)$ denotes the mean wave amplitude measured from the free surface and $A_i = \sqrt{2S_\zeta(\omega_i)\Delta\omega_i}$ denotes wave amplitude of each frequency component. In this expression, $\theta_i(t) = k_i x + \omega_i t + \varepsilon_i$, where t denotes the time, ω_i denotes the i^{th} frequency and ε_i denotes the i^{th} phase lag whose value is randomly assigned between 0 and 2π. Also $\Delta\omega_i$ is the i^{th} step size of the frequency. x denotes the position of the wave and k_i denotes i^{th} wave number. By taking the wave position (i.e $x_i = 0$ for all i) and following the same procedure, the heave force or pitch moment response spectra, shown in Figure 7, can be transformed to the

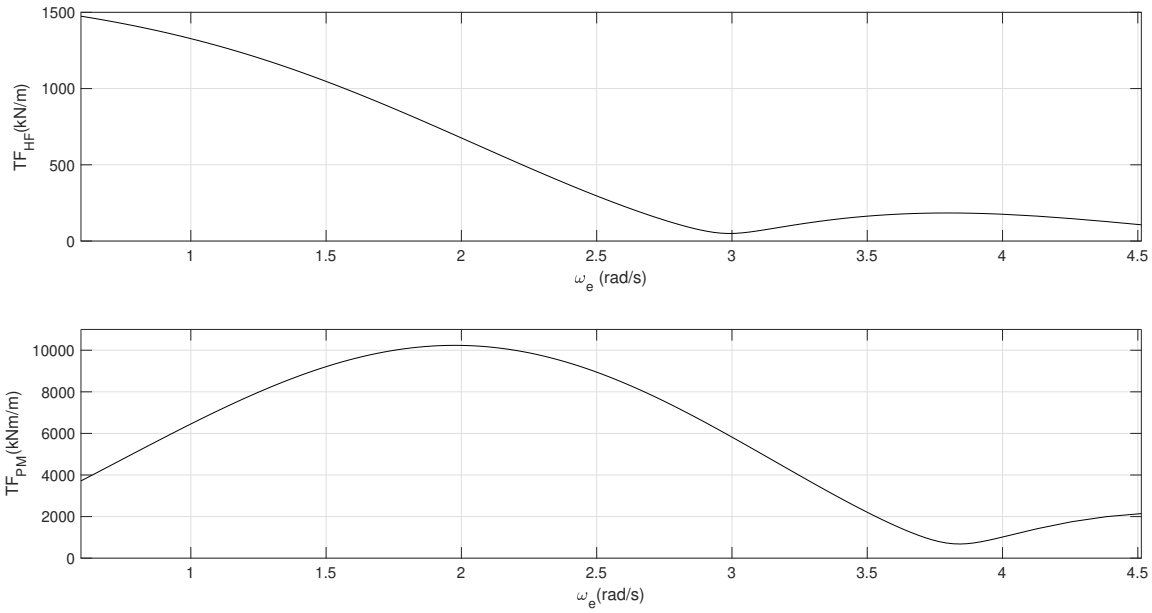

Figure 6: Heave force and pitch moment TF at $V = 10.288$m/s.

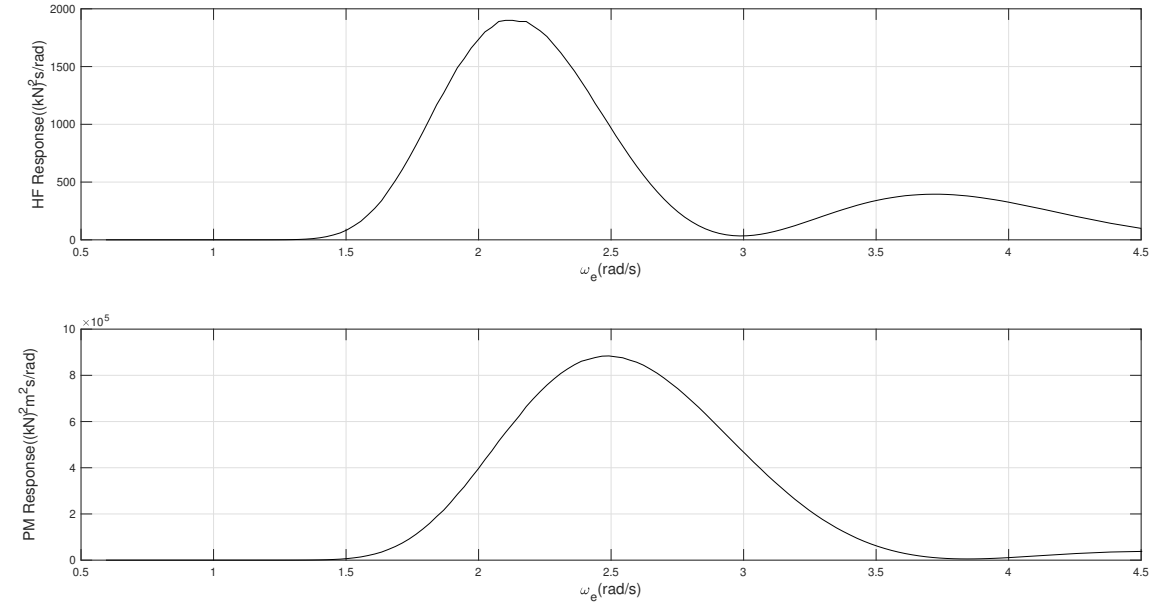

Figure 7: Heave Force-Pitch Moment Response Spectra representing $H_s = 0.88$ m. at $V = 10.288$m/s.

time domain as shown in Figure 8, for a simulation that lasts 100 seconds [5]. In this work, the number of regular wave components, N_i is taken as 132. Here, the number of components of regular waves are chosen

sufficiently enough to represent heave force and pitch moment due to wave-ship interactions.

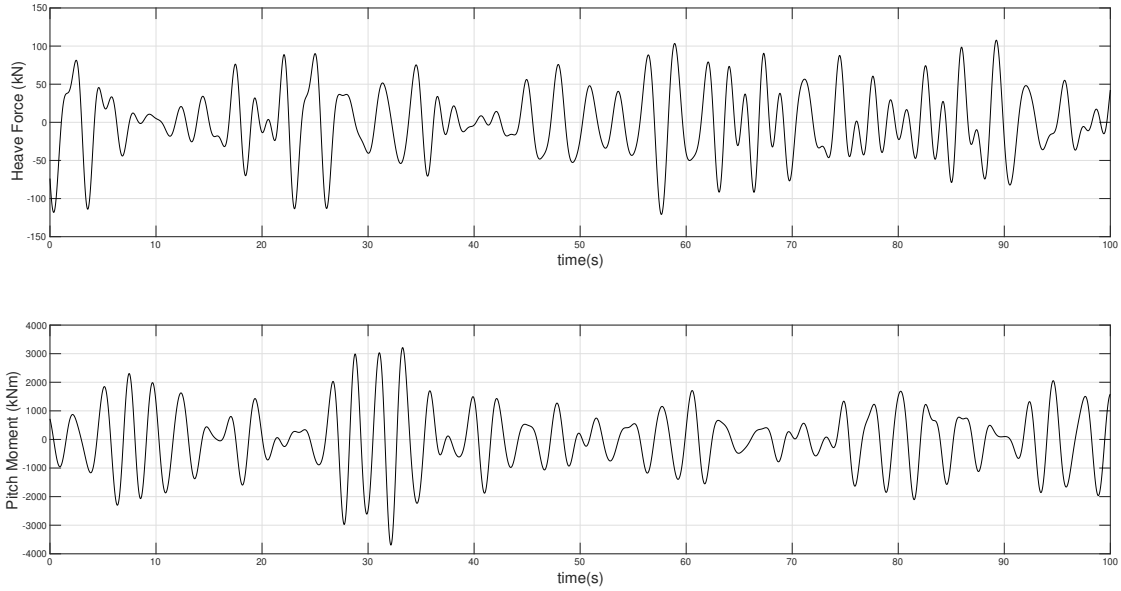

Figure 8: Heave Force and Pitch Moment in Time Domain at Hs=0.88 m.at $V = 10.288$m/s.

2.5. State Space Representation of Mathematical Model of Vertical Ship Motions and Actuator Equipped with Anti-Pitching foils

In this study, state-space representation is used to define the model of the system due to its multi-input and multi-output structure. The vertical motion of the ship can be represented as

$$\dot{x}(t) = Ax(t) + B_1[\text{wave}(t) - \text{conv}(t)] + B_2\alpha(t) \tag{19}$$

where $x(t) \in \mathbb{R}^n$ denotes the differentiable state vector, $\text{wave}(t) \in \mathbb{R}^{m_w}$ denotes the wave load input vector, $\text{conv}(t) \in \mathbb{R}^{m_w}$ denotes the convolution vector, and $\alpha(t) \in \mathbb{R}^{m_u}$ denotes the control input vector. A, B_1 and B_2 are known state-space matrices with appropriate dimensions. Using the change of variables, $x_1(t) \triangleq z_3(t)$, $x_2(t) \triangleq z_5(t)$, $x_3(t) \triangleq \dot{z}_3(t)$ and $x_4(t) \triangleq \dot{z}_5(t)$, the system matrices, disturbance input, control input and

states of the system can be obtained as follows:

$$A = \begin{bmatrix} 0_{2\times2} & I_2 \\ -M^{-1}R & -M^{-1}D \end{bmatrix}, B_1 = \begin{bmatrix} 0_{2\times2} \\ M^{-1} \end{bmatrix},$$

$$B_2 = \begin{bmatrix} & 0_{2\times2} & \\ 0.5 \times \rho \times V^2 \times (180/\pi) \times \begin{bmatrix} -1 & -1 \\ m_b & -m_s \end{bmatrix} & \begin{bmatrix} C_{\text{Lbow}} & 0 \\ 0 & C_{Lstern} \end{bmatrix} & \begin{bmatrix} S_{\text{bow}} & 0 \\ 0 & S_{stern} \end{bmatrix} \times M^{-1} \end{bmatrix},$$

$$\text{wave}(t) = \begin{bmatrix} F_3(t) \\ F_5(t) \end{bmatrix}, \alpha(t) = \begin{bmatrix} \alpha_{\text{bow}}(t) \\ \alpha_{\text{stern}}(t) \end{bmatrix}, \text{conv}(t) = \begin{bmatrix} \eta_1(t) \\ \eta_2(t) \end{bmatrix}, x(t) = \begin{bmatrix} x_1(t) & x_2(t) & x_3(t) & x_4(t) \end{bmatrix}^T \quad (20)$$

where, $x_1(t)$ denotes the heave motion, $x_2(t)$ stands for the pitch motion, $x_3(t)$ represents the heave velocity and $x_4(t)$ symbolises the pitch velocity. $F_3(t)$ denotes the heave force due to waves, $F_5(t)$ is used to represent the pitch moment due to waves. The terms aforementioned in the state-space matrices are as follows:

$$M = \begin{bmatrix} \bar{M} + A_{33}^{\infty} & A_{53}^{\infty} \\ A_{53}^{\infty} & \mathcal{I}_5 + A_{55}^{\infty} \end{bmatrix}, \quad R = \begin{bmatrix} C_{33} & C_{35} \\ C_{53} & C_{55} \end{bmatrix}, \quad D = \begin{bmatrix} B_{33}^{\infty} & B_{35}^{\infty} \\ B_{53}^{\infty} & B_{55}^{\infty} \end{bmatrix} \quad (21)$$

It should be noted that in B_2 matrix, moment arms m_b and m_s were taken as 19.25 metres from the bow

Table 1: Parameters of the ship model

Parameter (Unit)	Value
M (ton)	205
$\mathcal{I}_5$ (tonm^2)	23385
A_{33}^{∞} (ton)	214
A_{35}^{∞} (tonm)	560
A_{53}^{∞} (tonm)	568
A_{55}^{∞} (tonm^2)	19752
B_{33}^{∞} (ton/s)	153
B_{35}^{∞} (tonm/s)	2841
B_{53}^{∞} (tonm/s)	−630
B_{55}^{∞} (tonm^2/s)	27752
C_{33} (ton/s^2)	1566
C_{35} (tonm/s^2)	1287
C_{53} (tonm/s^2)	1287
C_{55} (tonm^2/s^2)	173322

and 16.80 metres from the stern with respect to centre of gravity. In addition to this, M denotes the mass matrix, R denotes the restoring matrix and D denotes the damping matrix. The passenger ship is equipped

with two submerged anti-pitching active foils. Table 1 summarizes the model parameters and their physical values used in this note. As shown in Figure 1, a pair of foils having symmetrical sections situated at bow and stern part of the ship to reduce the vertical motions. These foils are used to control vertical motions of the ship body in accordance to the control forces $U_{\text{bow}}(t)$ and $U_{\text{stern}}(t)$ computed by the real-time controller. Note that these actuators produce lift force as a function of ship speed V, effective angle of attacks, $\alpha_{\text{bow}}(t)$ and $\alpha_{\text{stern}}(t)$, projected area of the foils S_{bow} and S_{stern}, lift coefficients of the foils C_{Lbow} and C_{Lstern} and finally water density ρ. Note that in this work, S_{bow}=$S_{\text{stern}} = S$ and $C_{\text{Lbow}} = C_{\text{Lstern}} = C_L$. Then one can define

$$U_{\text{bow}}(t) \triangleq 0.5 \times \rho \times S_{\text{bow}} \times C_{\text{Lbow}} \times (180/pi) \times V^2 \times \alpha_{\text{bow}}(t) \tag{22}$$

$$U_{\text{stern}}(t) \triangleq 0.5 \times \rho \times S_{\text{stern}} \times C_{\text{Lstern}} \times (180/pi) \times V^2 \times \alpha_{\text{stern}}(t) \tag{23}$$

Hence, 22 and 23 can be used to transform the vertical forces $U_{\text{bow}}(t)$ and $U_{\text{stern}}(t)$ into effective foil angles, $\alpha_{\text{bow}}(t)$ and $\alpha_{\text{stern}}(t)$ assuming that the impact of the unsteady behaviour of lift characteristics is negligible. Here, the angle of attacks, $\alpha_{\text{bow}}(t)$ and $\alpha_{\text{stern}}(t)$ should be measured with respect to the parallel water flow. Therefore, the real angle of attacks can be expressed in terms of the online foil angle and the position of the ship as follows:

$$\alpha_{\text{bow}}(t) = \beta_{\text{bow}}(t) + x_2(t) + \theta_{\text{Fbow}}(t) \tag{24}$$

$$\alpha_{\text{stern}}(t) = \beta_{\text{stern}}(t) + x_2(t) + \theta_{\text{Fstern}}(t) \tag{25}$$

where, $\beta_{\text{bow}}(t)$ is the bow foil angle and $\beta_{\text{stern}}(t)$ is the stern foil angle of the ship. $\theta_{\text{Fbow}}(t)$ and $\theta_{\text{Fbow}}(t)$ depict the change the angle of attacks due to the online pitch and heave velocities of the ship and can be expressed as follows assuming that the arguments of the arctan functions vary in a very small interval:

$$\theta_{\text{Fbow}}(t) = \arctan\left(\frac{m_b \times x_4 - x_3 + \dot{\xi}}{V}\right) \cong \left(\frac{m_b \times x_4 - x_3 + \dot{\xi}}{V}\right) \tag{26}$$

$$\theta_{\text{Fstern}}(t) = \arctan\left(\frac{-m_s \times x_4 - x_3 + \dot{\xi}}{V}\right) \cong \left(\frac{-m_s \times x_4 - x_3 + \dot{\xi}}{V}\right) \tag{27}$$

Here, $\dot{\xi}$ stands for the heave velocity of wave on hydrofoil surface and its value is neglected since the foils are positioned sufficiently deep under mean water surface. Please note that there is also a contribution coming from the drag component due to the flow passing through the foil. However, this contribution may also be ignored since it is very small compared to the lift component.

Taking the foil opening angle $u(t) \triangleq \beta(t)$ as the the actual control input, the state-space equations of the vertical motion can be expressed as

$$\begin{aligned} \dot{x}(t) &= (A + B_2 B_3)x(t) + B_1[\text{wave}(t) - \text{conv}(t)] + B_2 u(t) \\ y(t) &= Cx(t) \end{aligned} \tag{28}$$

where

$$C = \begin{bmatrix} 0 & 1 & 0 & 0 \\ 0 & 0 & 0 & 1 \end{bmatrix}, \quad B_3 = \begin{bmatrix} 0 & 1 & -\frac{1}{V} & \frac{m_b}{V} \\ 0 & 1 & -\frac{1}{V} & -\frac{m_s}{V} \end{bmatrix} \tag{29}$$

All parameters that belong to the actuators are given in Table 2. In this paper, two identical active foils are used to actuate the system and their rotation angles are limited to $\pm 20\,\text{deg}$ ($\pm 0.349\,\text{rad}$), and rotation rates are limited to $\pm 20\,\text{deg/s}$ ($\pm 0.349\,\text{rad/s}$), due to mechanical restrictions of the actuators that drive foils [23]. On the other hand, it is well-know that the projected foil area is related to the water plane area of the ship and assessed according to a survey study for the cruise ships [23]. In this study, NACA 0021 hydrofoil is selected as the foil's section. Based on [24], Computational Fluid Dynamics (CFD) calculations gives 0.047 for the lift coefficient of NACA 0021 profile, having the aspect ratio $AR = 2$. This is obtained by fitting a linear curve to numerically calculated data.

Table 2: Parameters of the actuators

Parameters	Bow Foil	Stern Foil
Span (m)	1.866	1.866
Chord (m)	0.933	0.933
S (m^2)	1.742	1.742
AR (Span/Chord)(-)	2	2
Max. angle limit ($u_{\min}$, $u_{\max}$)(rad.)	± 0.349	± 0.349
Max. rotation rate limit (rad/s) ($u^d_{\min}$, $u^d_{\max}$)	± 0.349	± 0.349
$C_L(-)$	0.047	0.047
Distance to CoG (m_b and m_s) (m)	19.25	16.80

3. Disturbance Rejection Based Model Predictive Controller (MPC) Design

It is well known that input saturation, which can restrict the capability of actuators might cause remarkable performance degradation on the control system performance, sometimes even destabilization [25]. In many electro-mechanical applications including the active foil systems considered in this study, actuator can be saturated both in terms of the magnitude and the rate of change of the signal that is applied to the system. Therefore, the controllers that were designed by not considering these physical limitations cannot demonstrate the high performance that they exhibit in the simulation environment on the real system. Hence, in order to have a realistic and practically implementable controller, the design must consider the physical restrictions on both angle and the rate of the angle of foil. To overcome this issue, in this study, we propose an MPC strategy for the control of active foil system which is capable of eliminating the slowly varying disturbances such as waves by its integral type structure.

MPC is an advanced control strategy that is used to control complex processes while satisfying a set of constraints arising from the engaged system's characteristics. The main advantage of MPC is the fact that it allows the current timeslot to be optimally controlled, while keeping future behaviour of the system into account. This is achieved by optimizing a running finite time-horizon, but only modifying the current timeslot and then optimizing again, repeatedly, thus differing from any other offline optimal control method. The rest of this section investigates the design of an integral type multi-objective MPC that can be used in active foil control systems in ships.

Consider a linear discrete-time state-space model of the vertical motions of a ship governed by the following difference equations:

$$\begin{aligned} x_{k+1} &= \mathcal{A}x_k + \mathcal{B}u_k + \mathcal{B}_w w_k \\ y_k &= \mathcal{C}x_k + v_k \end{aligned} \tag{30}$$

where the subscripts refer to the sampling instants, $x_k \in \mathbb{R}^n$ is the state vector, $u_k \in \mathbb{R}^m$ is the control vector, $w_k \in \mathbb{R}^s$, is the disturbance signal having effect on the states, $v_k \in \mathbb{R}^p$ is the output disturbance and $y_k \in \mathbb{R}^p$ stands for the outputs. $\mathcal{A}$, $\mathcal{B}$, $\mathcal{B}_w$ and $\mathcal{C}$ are the system matrices obtained by discretising the continuous-time system having system matrices $A + B_2B_3$, B_2, B_1 and C, using a Zero-Order-Hold (ZOH) on the inputs and a sample time of T_s seconds, respectively. On the other hand, since the period of sea waves that affect the ship is much larger than the sampling time T_s, one can assume that the rate of change of the disturbance signals w_k and v_k are negligible, *i.e*, $w_k \simeq w_{k-1}$ and $v_k \simeq v_{k-1}$ for all $k \geq 0$. Hence, one can assume that $w_k = w$ and $v_k = v$ for all $k \geq 0$. Note that for discrete-time models used in control, there is normally no direct feed-through term $\mathcal{D}u_k$. Hence, the measurement y_k does not depend on the input at time k, but it depends on the input at time $k-1$ through the state x_k.

The control task of this note is to design an MPC strategy so that the output y_k follows a pre-defined reference input r_k as close as possible for all iterations k without violating the following component-wise control signal constraints:

$$u_{\min} \leq u_k \leq u_{\max}, \quad \forall\, 0 \leq k < N-1 \tag{31}$$

$$u^d_{\min} \leq \underbrace{u_k - u_{k-1}}_{\Delta u_k} \leq u^d_{\max}, \quad \forall\, 0 \leq k < N-1 \tag{32}$$

$u_{\min}$ stands for the lower bound of the control signal and $u_{\max}$ represents the upper bound of the control signal. $u^d_{\max}$ corresponds to the upper bound of the rate of the control signal whereas $u^d_{\min}$ denotes the lower bound for the rate of the control signal. For our case, the numerical values of these limits are shown in Table 2. Here, N is called the prediction horizon.

Hence, the optimisation problem can be stated as follows:

$$\underset{\Delta u_t,\ldots,\Delta u_{t+N-1}}{\text{minimise}} \quad J = \frac{1}{2}\|e_{t+N}\|_S^2 + \frac{1}{2}\sum_{k=0}^{N-1}\left(\|e_{t+k}\|_Q^2 + \|\Delta u_{t+k}\|_R^2\right) \tag{33}$$

where t represents the current time, J is the running cost function, $e_k \triangleq y_k - r_k$ stands for the tracking error; S, Q and R denote the symmetric positive definite constant weighting matrices with appropriate dimensions.

Our goal is to find out a suitable optimal MPC controller signal array $u^\star \in \mathbb{R}^{N\cdot m}$ that solves the optimisation problem (33) along with system trajectory (30) . Also the solution must satisfy the input constraints (31), (32) and capable of coping with the effects of slowly varying disturbances w and v on the states and the outputs, respectively. To achieve this goal, let us define a new augmented state vector $\tilde{x}_k \triangleq [\Delta x_k^T \quad y_{k-1}^T]^T$ where $\Delta x_k \triangleq x_k - x_{k-1}$. Hence,

$$\begin{aligned}
\Delta x_{k+1} &= x_{k+1} - x_k \\
&= \mathcal{A}x_k + \mathcal{B}u_k + \mathcal{B}_w w - \mathcal{A}x_{k-1} - \mathcal{B}u_{k-1} - \mathcal{B}_w w \\
&= \mathcal{A}(x_k - x_{k-1}) + \mathcal{B}\underbrace{(u_k - u_{k-1})}_{\Delta u_k} \\
&= \mathcal{A}\Delta x_k + \mathcal{B}\Delta u_k
\end{aligned} \tag{34}$$

Similarly,

$$\begin{aligned}
y_k - y_{k-1} &= \mathcal{C}x_k + v - \mathcal{C}x_{k-1} - v \\
y_k &= \mathcal{C}\Delta x_k + y_{k-1}
\end{aligned} \tag{35}$$

Then, for the sampling instant k, one can define the following augmented state and output equations which are reliant on the rate of change of the control signal Δu_k.

$$\begin{aligned}
\begin{bmatrix}\Delta x_{k+1}\\ y_k\end{bmatrix} &= \underbrace{\begin{bmatrix}\mathcal{A} & 0_{n\times p}\\ \mathcal{C} & I_p\end{bmatrix}}_{\tilde{A}}\underbrace{\begin{bmatrix}\Delta x_k\\ y_{k-1}\end{bmatrix}}_{\tilde{x}_k} + \underbrace{\begin{bmatrix}\mathcal{B}\\ 0_{p\times m}\end{bmatrix}}_{\tilde{B}}\Delta u_k \\
y_k &= \underbrace{\begin{bmatrix}\mathcal{C} & I_p\end{bmatrix}}_{\tilde{C}}\underbrace{\begin{bmatrix}\Delta x_k\\ y_{k-1}\end{bmatrix}}_{\tilde{x}_k}
\end{aligned} \tag{36}$$

It is also obvious from these equations that the new augmented state-space system is independent of the disturbances, w and v. Then, using the definitions

$$r \triangleq \begin{bmatrix} r_{t+1}\\ \vdots \\ r_{t+N}\end{bmatrix} \in \mathbb{R}^{N\cdot p}\ , \tilde{x} \triangleq \begin{bmatrix}\tilde{x}_{t+1}\\ \vdots \\ \tilde{x}_{t+N}\end{bmatrix} \in \mathbb{R}^{N\cdot(n+p)},\ \Delta u \triangleq \begin{bmatrix}\Delta u_t\\ \vdots \\ \Delta u_{t+N-1}\end{bmatrix} \in \mathbb{R}^{N\cdot m} \tag{37}$$

one can write the prediction equation as follows:

$$\tilde{x} = \bar{C}\Delta u + \bar{A}\tilde{x}_t \tag{38}$$

where

$$\bar{C} = \begin{bmatrix} \tilde{B} & 0 & \cdots & 0 \\ \tilde{A}\tilde{B} & \tilde{B} & \cdots & 0 \\ \vdots & \vdots & \ddots & \vdots \\ \tilde{A}^{N-1}\tilde{B} & \tilde{A}^{N-2}\tilde{B} & \cdots & \tilde{B} \end{bmatrix}, \quad \bar{A} = \begin{bmatrix} \tilde{A} \\ \tilde{A}^2 \\ \vdots \\ \tilde{A}^N \end{bmatrix} \tag{39}$$

Hence, in the light of these definitions, the optimisation problem (33) can be rewritten as

$$\underset{\Delta u}{\text{minimise}} \;\; J = \frac{1}{2}\Delta u^T H \Delta u + \begin{bmatrix} \tilde{x}_t^T & r^T \end{bmatrix} F \Delta u \tag{40}$$

where

$$H = \bar{C}^T \bar{Q} \bar{C} + \bar{R} \tag{41}$$

$$F = \begin{bmatrix} \bar{A}^T \bar{Q} \bar{C} \\ \\ -T\bar{C} \end{bmatrix} \tag{42}$$

$$\bar{Q} = \left.\begin{bmatrix} \tilde{C}^T Q \tilde{C} & & & \\ & \ddots & & \\ & & \tilde{C}^T Q \tilde{C} & \\ & & & \tilde{C}^T S \tilde{C} \end{bmatrix}\right\} N-1 \text{ times} \tag{43}$$

$$T = \left.\begin{bmatrix} Q\tilde{C} & & & \\ & \ddots & & \\ & & Q\tilde{C} & \\ & & & S\tilde{C} \end{bmatrix}\right\} N-1 \text{ times}, \quad \text{and} \quad \bar{R} = \left.\begin{bmatrix} R & & & \\ & R & & \\ & & \ddots & \\ & & & R \end{bmatrix}\right\} N \text{ times} \tag{44}$$

Here, H is called the Hessian matrix which needs to be always positive definite. In order to utilise (40) in the MPC design, the control constraints (31) and (32) must also be defined in terms of the decision variable Δu.

Note that

$$\begin{bmatrix} u_t \\ u_{t+1} \\ \vdots \\ u_{t+N-1} \end{bmatrix} = \underbrace{\begin{bmatrix} I_m \\ I_m \\ \vdots \\ I_m \end{bmatrix}}_{\tilde{I}_m} u_{t-1} + \underbrace{\begin{bmatrix} I_m & 0 & \cdots & 0 \\ I_m & I_m & \cdots & 0 \\ \vdots & \vdots & \ddots & \vdots \\ I_m & I_m & \cdots & I_m \end{bmatrix}}_{\Omega_1} \underbrace{\begin{bmatrix} \Delta u_t \\ \Delta u_{t+1} \\ \vdots \\ \Delta u_{t+N-1} \end{bmatrix}}_{\Delta u} \tag{45}$$

Hence, (31) can be replaced with

$$\begin{bmatrix} \Omega_1 \\ \\ -\Omega_1 \end{bmatrix} \Delta u \leq \begin{bmatrix} U_{\text{MAX}} \\ \\ -U_{\text{MIN}} \end{bmatrix} - \begin{bmatrix} \tilde{I}_m \\ \\ -\tilde{I}_m \end{bmatrix} u_{t-1} \tag{46}$$

where

$$U_{\text{MAX}} = \begin{bmatrix} u_{\max} \\ \vdots \\ u_{\max} \end{bmatrix} \in \mathbb{R}^{N \cdot m}, \quad U_{\text{MIN}} = \begin{bmatrix} u_{\min} \\ \vdots \\ u_{\min} \end{bmatrix} \in \mathbb{R}^{N \cdot m} \tag{47}$$

On the other hand, it is also possible to put physical constraints on how fast the inputs can change. The input rate of movement is the amount of control signal that changes when the iteration moves from sample $k-1$ to k and therefore is called Δu_k. The constraints can be directly written as

$$U^d_{\text{MIN}} \leq \Delta u_k \leq U^d_{\text{MAX}}, \qquad \forall k \in \{t, \ldots, t+N-1\} \tag{48}$$

where

$$U^d_{\text{MAX}} = \left.\begin{bmatrix} u^d_{\max} \\ \vdots \\ u^d_{\max} \end{bmatrix}\right\} \in \mathbb{R}^{N \cdot m} \quad \text{and} \quad U^d_{\text{MIN}} = \left.\begin{bmatrix} u^d_{\min} \\ \vdots \\ u^d_{\min} \end{bmatrix}\right\} \in \mathbb{R}^{N \cdot m} \tag{49}$$

which implies

$$\begin{bmatrix} I_{N \cdot m} \\ \\ -I_{N \cdot m} \end{bmatrix} \Delta u \leq \begin{bmatrix} U^d_{\text{MAX}} \\ \\ -U^d_{\text{MIN}} \end{bmatrix} \tag{50}$$

Assuming that a full measurement of the state x_t is available at the current time t, the following finite-horizon optimal tracking problem is solved at every time instant t to find the optimal control sequence $\Delta u^\star$:

$$\begin{aligned} \underset{\Delta u}{\text{minimise}} \quad & \tfrac{1}{2} \Delta u^T H \Delta u + \begin{bmatrix} \tilde{x}_t^T & r^T \end{bmatrix} F \Delta u \\ \text{subject to} \quad & \begin{cases} \begin{bmatrix} \Omega_1 \\ \\ -\Omega_1 \end{bmatrix} \Delta u \leq \begin{bmatrix} U_{\text{MAX}} \\ \\ -U_{\text{MIN}} \end{bmatrix} - \begin{bmatrix} \tilde{I}_m \\ \\ -\tilde{I}_m \end{bmatrix} u_{t-1} \\ \\ \begin{bmatrix} I_{N \cdot m} \\ \\ -I_{N \cdot m} \end{bmatrix} \Delta u \leq \begin{bmatrix} U^d_{\text{MAX}} \\ \\ -U^d_{\text{MIN}} \end{bmatrix} \end{cases} \end{aligned} \tag{51}$$

Once a feasible solution $\Delta u^\star$ to the quadratic optimisation problem (51) is obtained, only the first m entries of the signal is used as a control signal for the system (30). Thus, the control signal at time t can be obtained

as

$$u_t = u_{t-1} + \Delta u_t \tag{52}$$

The satisfaction of the predictive control is highly influenced by the choice of the sampling period, T_s, prediction horizon N and the control horizon N_u. A recommended practice is to choose T_s between 10% and 25% of the minimum desired closed-loop response time. Qualitatively, as T_s decreases, the satisfaction of the attenuation of the disturbance w usually improves and then does not change much. But, as T_s becomes small, the computational effort increases dramatically due to the need for an increase in N. Thus, the optimal choice for T_s is a trade-off between performance and computational effort.

In MPC, the choice of the prediction horizon, N is also an important consideration. It is the number of predicted future time steps and shows how far the controller predicts into the future. If one chooses to hold the prediction horizon duration ($N \times T_s$) constant, N must vary inversely with T_s. As can be seen above, many array sizes are proportional to N. Thus, as N increases, the controller memory requirements and quadratic programming solution time increase.

Another design parameter is the control horizon, N_u. It is the number of non-zero control actions that can be used to keep the system's output in the predicted horizon. Each control move in the control horizon can be thought of as a free variable that needs to be computed by the optimizer. However, it is not a reasonable approach to set $N_u = N$, since only the first few steps are dominant on the response of the system. Hence, it is a common practice to keep N_u as small as possible and set $u_k = 0$ for $N_u + 1 \leq k \leq N$ since, smaller the control horizon, the fewer the computations we have.

In this work, based on the dynamics of the open-loop system, the sampling period is chosen as $T_s = 0.01$ seconds. Also, through a trial and error approach, it is seen that the best performance is obtained for the design parameters $N = 150$ and $N_u = 2$.

In this note, when $F_n = 0.5$, using a Zero Order Hold type discretization, one can obtain the system matrices as follows:

$$\mathcal{A} = \begin{bmatrix} 0.9998 & 0.0001 & 0.0100 & -0.0003 \\ 0.0000 & 0.9998 & 0.0000 & 0.0100 \\ -0.0378 & 0.0122 & 0.9971 & -0.0669 \\ 0.0002 & -0.0401 & 0.0002 & 0.9980 \end{bmatrix}, \quad \mathcal{B}_w = 10^{-4} \times \begin{bmatrix} 0.0012 & 0.0000 \\ 0.0000 & 0.0000 \\ 0.2439 & -0.0032 \\ -0.0032 & 0.0024 \end{bmatrix}$$

$$\mathcal{B} = \begin{bmatrix} 0 & 0 \\ 0 & 0 \\ -0.0078 & -0.0048 \\ 0.0012 & -0.0009 \end{bmatrix}, \quad \mathcal{C} = \begin{bmatrix} 0 & 1 & 0 & 0 \\ 0 & 0 & 0 & 1 \end{bmatrix} \tag{53}$$

For $F_n = 0.4$, we have the same system matrices given in (54) except

$$\mathcal{A} = \begin{bmatrix} 0.9998 & 0.0001 & 0.0100 & -0.0003 \\ 0.0000 & 0.9998 & 0.0000 & 0.0100 \\ -0.0378 & 0.0167 & 0.9969 & -0.0656 \\ 0.0002 & -0.0402 & 0.0002 & 0.9972 \end{bmatrix}, \quad \mathcal{B} = \begin{bmatrix} 0 & 0 \\ 0 & 0 \\ -0.0050 & -0.0031 \\ 0.0008 & -0.0006 \end{bmatrix} \tag{54}$$

On the other hand, during the design of MPC, weighting matrices of the objective function are chosen as follows: $S = \text{diag}\{100, 100\}$, $Q = \text{diag}\{1, 1\}$ and $R = \text{diag}\{0.1, 0.1\}$ both for $F_n = 0.4$ and $F_n = 0.5$. Finally, the reference trajectory is chosen to be $r = 0 \in \mathbb{R}^{300}$ for very iteration k.

4. Discrete-time $\mathcal{H}_\infty$ state-feedback control for systems having magnitude and rate-saturated actuators

In this section, to demonstrate the efficiency of the proposed MPC strategy and to provide a fair comparison with MPC approach, derivation of a novel optimal state-feedback $\mathcal{H}_\infty$ controller for discrete-time systems having amplitude and rate limited actuators is considered.

Assume that the vertical motions of a ship are governed by the difference equations (30). Also, assume that the system is subject to control constraints defined by (31) and (32). Note that the control action can be modelled in state-space as

$$u_k = I_m u_{k-1} + I_m \Delta u_k \tag{55}$$

Then, the augmented state-space system can be written as

$$\begin{aligned} \bar{x}_{k+1} &= \underbrace{\begin{bmatrix} \mathcal{A} & \mathcal{B} \\ 0_{m\times n} & I_m \end{bmatrix}}_{\mathbb{A}} \underbrace{\begin{bmatrix} x_k \\ u_{k-1} \end{bmatrix}}_{\bar{x}_k} + \underbrace{\begin{bmatrix} \mathcal{B} \\ I_m \end{bmatrix}}_{\mathbb{B}} \Delta u_k + \underbrace{\begin{bmatrix} \mathcal{B}_w \\ 0_{m\times s} \end{bmatrix}}_{\mathbb{B}_w} w_k \\ y_k &= \underbrace{\begin{bmatrix} \mathcal{C} & 0_{p\times m} \end{bmatrix}}_{\mathbb{C}} \bar{x}_k \end{aligned} \tag{56}$$

Denoting the transfer function from w to y by $\mathcal{T}_{wy}$, the following theorem provides an optimal static state-feedback $\mathcal{H}_\infty$ control law for the augmented system (56).

Theorem 1. *There exists a static state-feedback controller in the form of*

$$u_k = u_{k-1} + \underbrace{\mathcal{M}\mathcal{X}^{-1}}_{\mathcal{K}} \bar{x}_k \tag{57}$$

such that the inequality $\|\mathcal{T}_{wy}\|_\infty < \gamma$ holds if and only if there exist a symmetric matrix $\mathcal{X}$, and a matrix $\mathcal{M}$ of appropriate dimensions such that the following Linear Matrix Inequalities(LMIs) hold:

$$\begin{bmatrix} \mathcal{X} & 0 & \star & \star \\ 0 & \gamma I_s & \star & 0 \\ \mathbb{A}\mathcal{X} + \mathbb{B}\mathcal{M} & \mathbb{B}_w & \mathcal{X} & 0 \\ \mathbb{C}\mathcal{X} & 0 & 0 & \gamma I_p \end{bmatrix} \succeq 0 \tag{58}$$

and

$$\begin{bmatrix} \mathcal{X} & \mathcal{M}_i^T \\ \mathcal{M}_i & (u^d_{i,\max})^2 \end{bmatrix} \succeq 0, \qquad \begin{bmatrix} \mathcal{X} & \mathcal{X}L_{n+i}^T \\ \star & \left(u_{i,\max} - u^d_{i,\max}\right)^2 \end{bmatrix} \succeq 0 \tag{59}$$

for all $i = 1, \ldots, m$ where $\mathcal{M}_i$ is the i-th row of $\mathcal{M}$ and L_{n+i} is a row vector whose $(n+i)$-th entry is 1 and all other entries are 0. Finally, $u_{i,\max}$ is the i-th row of the vector $u_{\max}$ and $u^d_{i,\max}$ is the i-th row of the vector $u^d_{\max}$.

PROOF. Consider a Lyapunov functional of the form $V_k = \bar{x}_k^T \mathcal{X}^{-1} \bar{x}_k$ at time instant k along the system trajectory (56). Assume that the augmented system is controlled by a control signal of the form $\Delta u_k = \mathcal{K}\bar{x}_k$. It is easy to show that if

$$V_{k+1} - V_k + \frac{1}{\gamma} y_k^T y_k - \gamma w_k^T w_k \leq 0 \tag{60}$$

then $\|\mathcal{T}_{wy}\|_\infty \triangleq \mathbf{sup}_{w \neq 0} \frac{\|y\|_2}{\|w\|_2} < \gamma$. According to Bounded-Real Lemma [26], this inequality is equivalent to

$$\begin{bmatrix} \mathcal{X}^{-1} & 0 & \star & \star \\ 0 & \gamma I_s & \star & 0 \\ \mathcal{X}^{-1}\mathbb{A} + \mathcal{X}^{-1}\mathbb{B}\mathcal{K} & \mathcal{X}^{-1}\mathbb{B}_w & \mathcal{X}^{-1} & 0 \\ \mathbb{C} & 0 & 0 & \gamma I_p \end{bmatrix} \succeq 0 \tag{61}$$

Applying a congruence transformation by pre- and post multiplying (61) with $\mathbf{diag}\{\mathcal{X}, I, \mathcal{X}, I\}$ and defining $\mathcal{M} \triangleq \mathcal{K}\mathcal{X}$ yields (58).

On the other hand, let $\Delta u_{i,k}$ denotes the i-th entry of the rate-of-control signal at time instant k. From the slew-rate requirements of the control signal, $|\Delta u_{i,k}| \leq u^d_{i,\max}$ must to be satisfied for all $k \geq 0$ and $i = 1, \ldots, m$. Note that this inequality is equivalent to $\Delta u_{i,k}^2 \leq \left(u^d_{i,\max}\right)^2$ which can be further written as

$$\bar{x}_k^T \mathcal{K}_i^T \mathcal{K}_i \bar{x}_k \leq \left(u^d_{i,\max}\right)^2, \qquad i = 1, \ldots, m \tag{62}$$

where $\mathcal{K}_i$ stands for the $i-$th row of the feedback matrix $\mathcal{K}$. Rate constraints can be satisfied if the ellipsoid

$$\mathbf{Elp}\left(\frac{\mathcal{K}_i^T \mathcal{K}_i}{\left(u^d_{i,\max}\right)^2}\right) \triangleq \bar{x}_k^T \frac{\mathcal{K}_i^T \mathcal{K}_i}{\left(u^d_{i,\max}\right)^2} \bar{x}_k \leq 1 \tag{63}$$

contains the closed-loop system's energy ellipsoid $\bar{x}_k^T \mathcal{X}^{-1} \bar{x}_k \leq 1$ for all $k \geq 0$. From the theory of ellipsoids 26, this can only happen when

$$\frac{\mathcal{K}_i^T \mathcal{K}_i}{\left(u_{i,\max}^d\right)^2} \preceq \mathcal{X}^{-1}, \qquad i = 1, \ldots, m \tag{64}$$

Pre- and post multiplying both sides of the (64) by $\mathcal{X}$ and using the definition $\mathcal{K}\mathcal{X} = \mathcal{M}$ yields

$$\frac{\mathcal{M}_i^T \mathcal{M}_i}{\left(u_{i,\max}^d\right)^2} \preceq \mathcal{X}, \qquad i = 1, \ldots, m \tag{65}$$

Finally, using Schur complement formula [26] on (65) gives the first LMI in (59).

Similarly, let us denote the i-th entry of the control vector u_k by $u_{i,k}$. The control signal should satisfy $|u_{i,k}| \leq u_{i,\max}$ for all $k \geq 0$ and $i = 1, \ldots, m$ which is equivalent to $u_{i,k}^2 \leq \left(u_{i,\max}\right)^2$. However, since the control system do not have access to u_k at sampling time k, but u_{k-1}, one can consider a bound $|u_{i,k-1}| \leq u_{i,\max} - u_{i,\max}^d$ for all $k \geq 0$ and $i = 1, \ldots, m$. This can be further described as an ellipsoid of the form

$$\mathbf{Elp}\left(\frac{L_{n+i}^T L_{n+i}}{\left(u_{i,\max} - u_{i,\max}^d\right)^2}\right) \triangleq \bar{x}_k^T \frac{L_{n+i}^T L_{n+i}}{\left(u_{i,\max} - u_{i,\max}^d\right)^2} \bar{x}_k \leq 1 \tag{66}$$

So, magnitude constraints on the control signal can be satisfied at all times if

$$\mathbf{Elp}\left(\frac{L_{n+i}^T L_{n+i}}{\left(u_{i,\max} - u_{i,\max}^d\right)^2}\right) \preceq \mathcal{X}^{-1}, \qquad i = 1, \ldots, m \tag{67}$$

Pre- and post multiplying both sides of the (67) by $\mathcal{X}$ and using Schur complement formula [26] yields the second LMI given in (59). This concludes the proof. ■

5. Simulation Study

In this section, the results of the simulation studies which were performed for mitigating the vertical accelerations of the passenger ship in irregular head waves having Froude number $F_n = \frac{V}{\sqrt{gL_{WL}}} = 0.40$ and 0.50 are presented with the help of several tables and graphs. The optimisation problem (51) is solved in real time for a suitable MPC using the system matrices given in (54). All computations are accomplished using MATLAB along with `quadprog` solver by taking all initial conditions equal to zero. Each simulation representing $H_s = 0.70$, 0.88 and 1.00 metres at $F_n = 0.40$ and $F_n = 0.50$ last 100 seconds. In order to compare the performance of the proposed MPC with another optimal control method, discrete time $\mathcal{H}_\infty$ state feedback controller has been performed for the modelled passenger ship under consideration of magnitude and rate saturated foils.

During the simulation study, an $\mathcal{H}_\infty$ controller gain

$$\mathcal{K} = \begin{bmatrix} 0.0007 & 0.1905 & -0.0024 & -0.0351 & -0.0042 & 0.0035 \\ -0.0020 & -0.1776 & 0.0019 & 0.0102 & 0.0036 & -0.0033 \end{bmatrix} \tag{68}$$

is used for $F_n = 0.4$, and

$$\mathcal{K} = \begin{bmatrix} -0.0175 & -3.5550 & -0.0160 & -9.3183 & -0.1187 & 0.0891 \\ 0.0173 & 3.9295 & 0.0161 & 9.2341 & 0.1191 & -0.0900 \end{bmatrix} \tag{69}$$

for $F_n = 0.5$. These controller gains are obtained by solving the LMIs given in (58) and (59) using YALMIP [27] with SeduMi solver in MATLAB. Time-domain comparison of uncontrolled and controlled states (MPC and $\mathcal{H}_\infty$) and vertical accelerations at the bow, stern and central locations of the ship for $F_n = 0.40$ are given in Figure 9 - Figure 14 for $H_s = 0.70$, 0.88 and 1.00 metres, respectively.

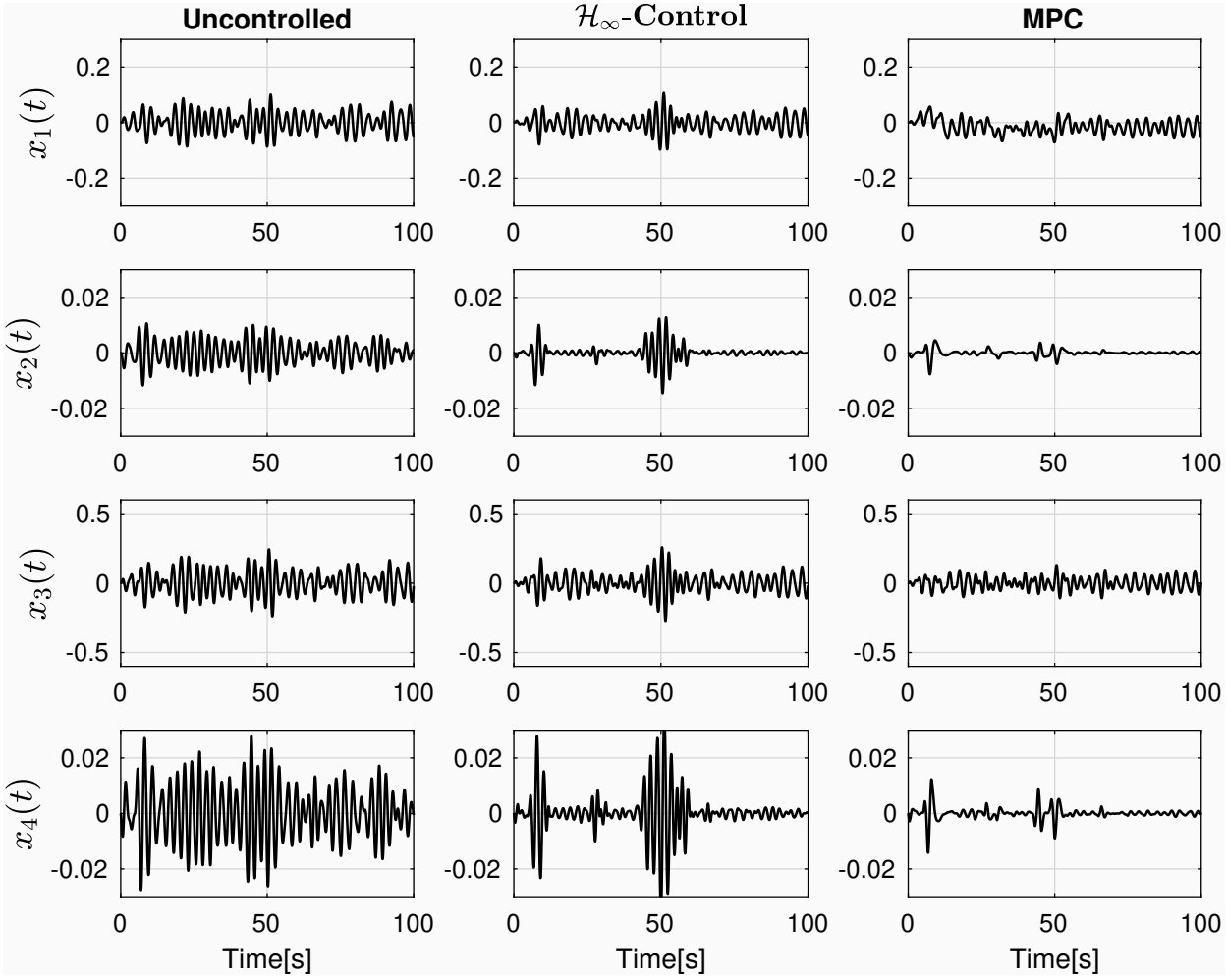

Figure 9: Time histories of uncontrolled and controlled states at $F_n = 0.40$ ($H_s = 0.70$m).

Similarly, time-domain comparison of uncontrolled and controlled states (MPC and $\mathcal{H}_\infty$) and vertical accelerations at the bow, stern and central locations of the ship for $F_n = 0.50$ are provided in Figure 15 - Figure 20 for $H_s = 0.70$, 0.88 and 1.00 metres, respectively. Figures 9-Figure 20 reveal that the MPC design is very successful in reducing pitch motion and pitch velocity for two forward ship speeds even in higher

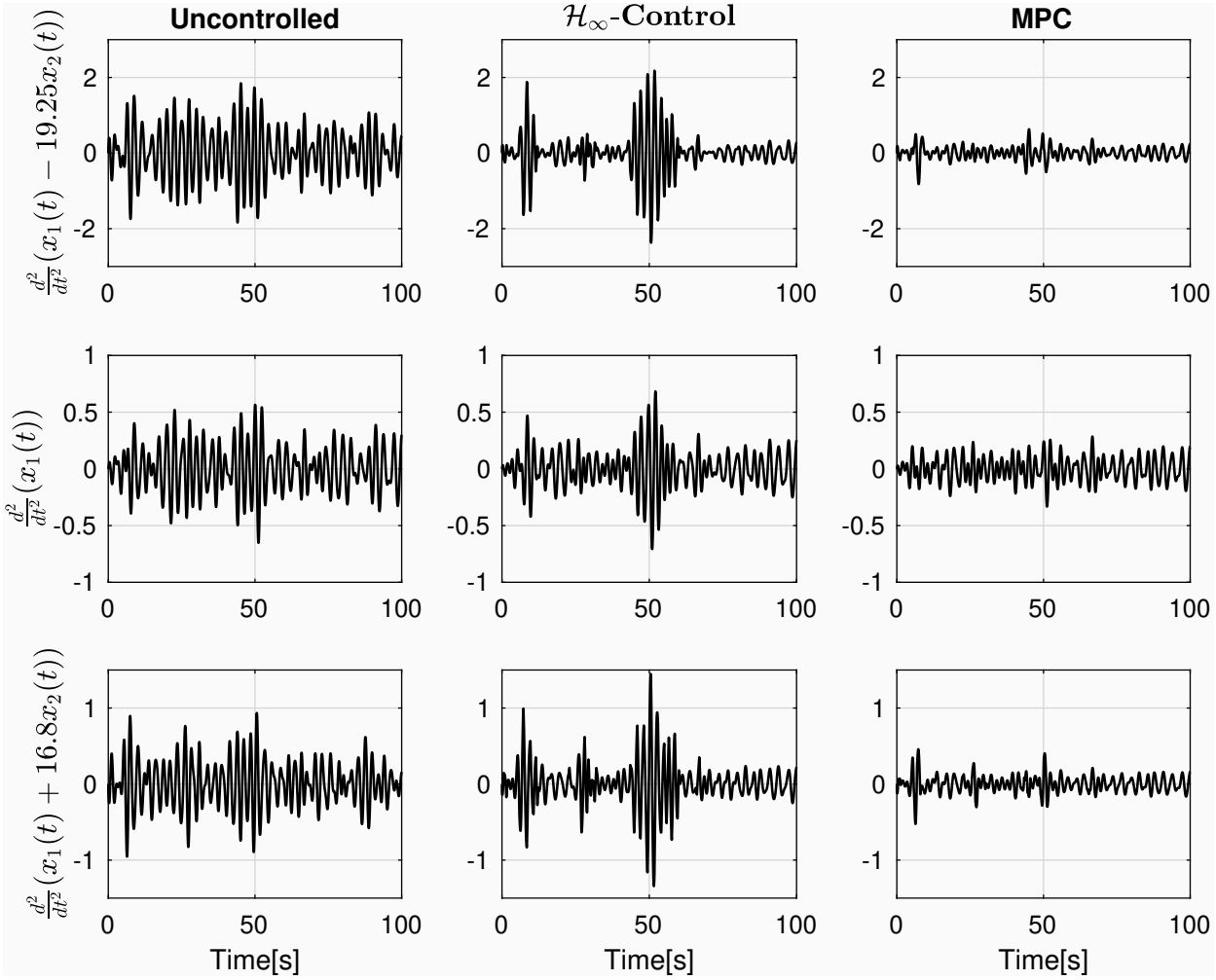

Figure 10: Time histories of uncontrolled and controlled accelerations at $F_n = 0.40$ ($H_s = 0.70$m).

sea states. In conjunction with the improvements in pitch motion and pitch velocity of the passenger ship, bow and stern accelerations are reduced remarkably as well particularly in $H_s = 0.70$ metres significant wave height. It is also noted that the attenuations of the heave acceleration are less than the attenuation of the bow and stern accelerations due to the phase difference between the pitch and heave motions. In other words, only heave or pitch motion can be attenuated with a high level of efficiency. As known, the consideration of the seasickness index of the passengers who sit at bow and stern are more important since the motion is larger at bow and stern than center. Therefore, in this study, it is aimed to reduce preferably pitch motion and velocity rather than heave motion and velocity.

On the other hand, the control signals for the real foil angles $\beta(t)$ and their rates $\dot{\beta}(t)$ at $F_n = 0.40$ are given in Figure 21, Figure 22 and Figure 23 in corresponding sea sates. In the same way, the control signals for the real foil angles $\beta(t)$ and their rates $\dot{\beta}(t)$ at $F_n = 0.50$ are given in Figure 24, Figure 25 and

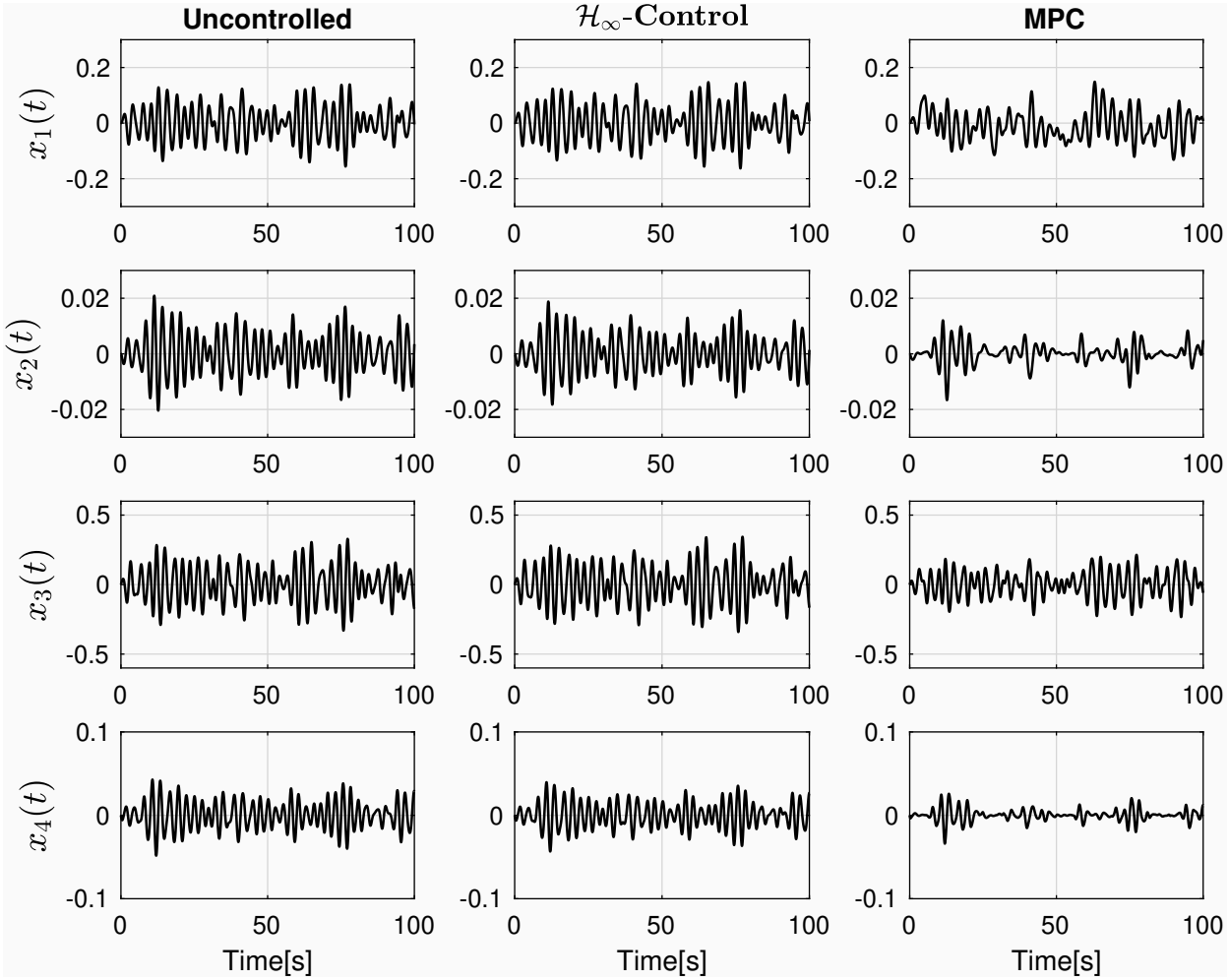

Figure 11: Time histories of uncontrolled and controlled states at $F_n = 0.40$ ($H_s = 0.88$ m).

Figure 26 in corresponding sea sates. As it can be seen from the figures, both the foil angles and their rates are remained within the limits of actuator opening angle (20deg, 20deg) and (20deg/s, 20deg/s) rate of opening angles at all times for $F_n = 0.40$ and $F_n = 0.50$.

In Table 3 - Table 5, the responses at $F_n = 0.40$ are tabulated with uncontrolled and controlled responses of the passenger ship under the disturbance corresponding to $H_s = 0.70$, 0.88 and 1.00 metres, respectively. In Table 6 - Table 8, the responses at $F_n = 0.50$ are tabulated with uncontrolled and controlled responses of the passenger ship under the disturbance corresponding to $H_s = 0.70$, 0.88 and 1.00 metres, respectively.

As it is readily seen from Table 3 - Table 8, conducted simulation studies show that the designed MPC controller has better performance than $\mathcal{H}_\infty$ controller. The underlying reason behind this is, MPC has advantages in a wave attenuation problem with its preview capability of wave disturbances and handling the foil angle and rate of foil angle constraints. Therefore, Table 9 and Table 10 summarise the acceleration

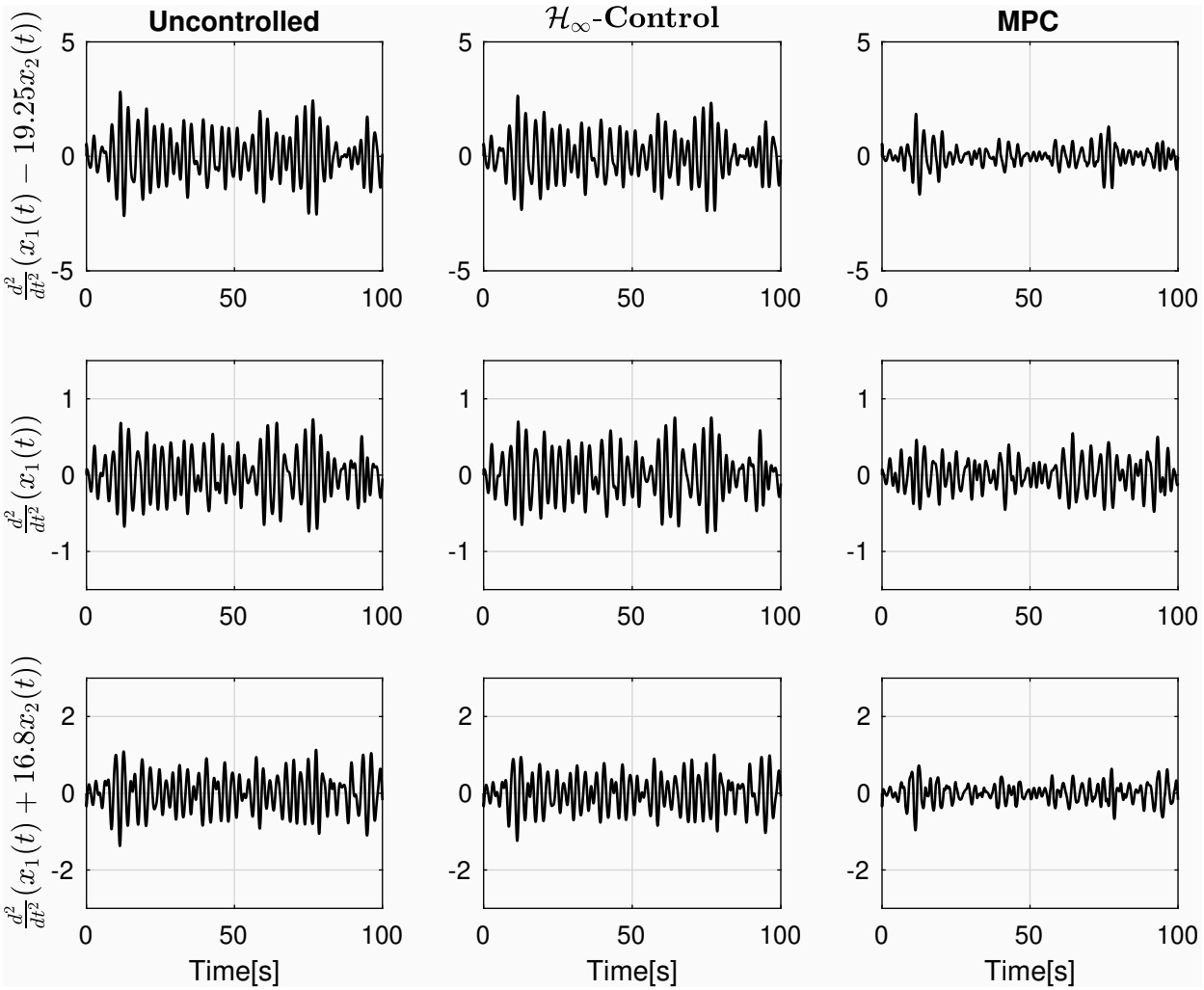

Figure 12: Time histories of uncontrolled and controlled accelerations at $F_n = 0.40$ ($H_s = 0.88$ m).

Table 3: Uncontrolled and controlled vertical responses at $F_n = 0.40$ ($H_s = 0.70$ metres).

	Uncontrolled	Controlled ($\mathcal{H}_\infty$)	Controlled (MPC)
Pitch Motion (rms) (radians)	0.00425	0.00282	0.00117
Bow Vertical Acceleration (rms) (m/s^2)	0.6806	0.5077	0.1695
Stern Vertical Acceleration (rms) (m/s^2)	0.3085	0.2878	0.1111
CoG Acceleration (rms) (m/s^2)	0.2085	0.1719	0.1072

reduction capabilities of MPC for $F_n = 0.40$ and $F_n = 0.50$. As seen from Table 9 and Table 10, the designed MPC controller is generally more effective at $F_n = 0.50$ since the advance speed of the ship affects the control input matrices quadratically. It is interesting to note that the excitation terms are also different at different Froude numbers when the ship is exposed to the same wave spectrum. Therefore, the efficiency

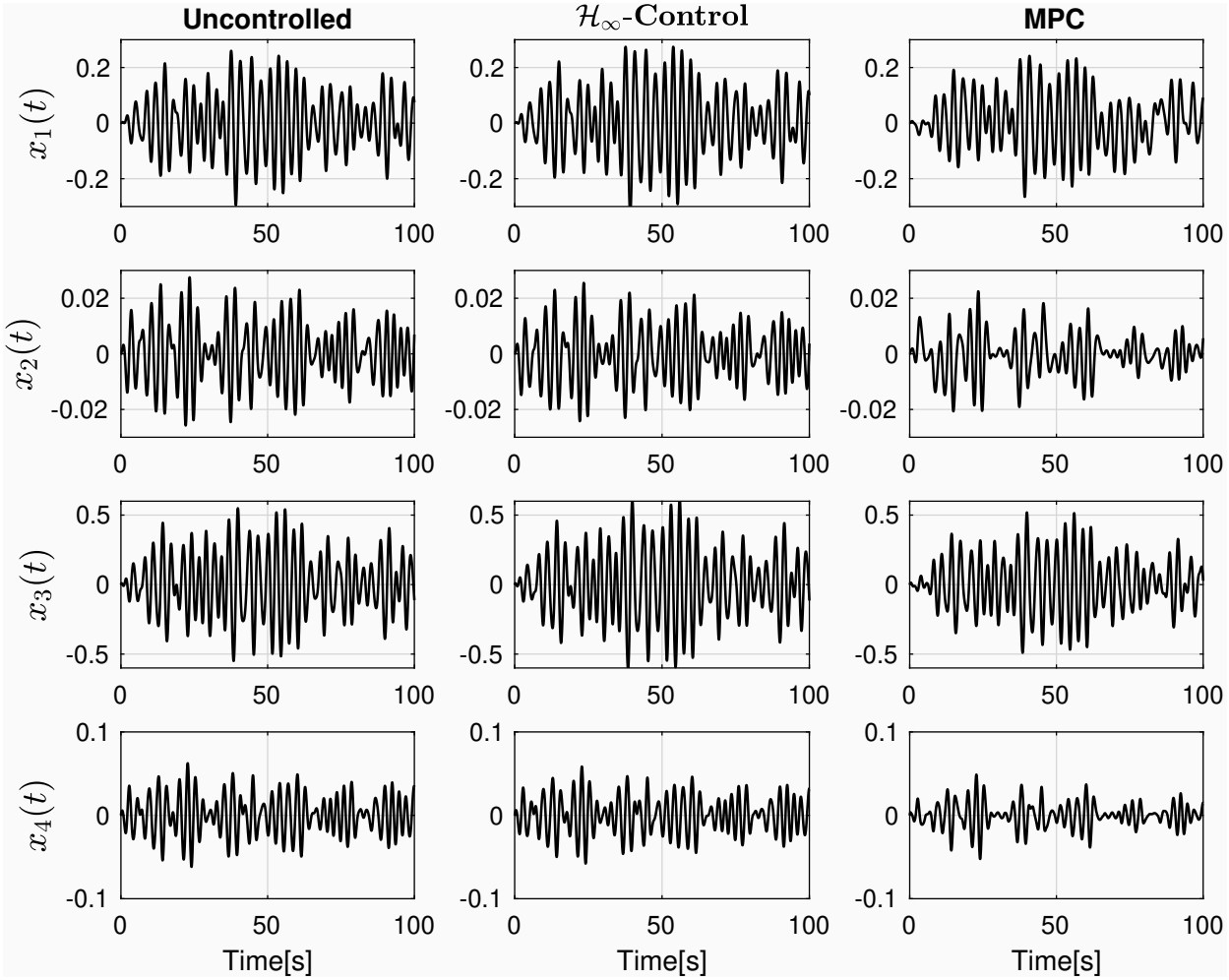

Figure 13: Time histories of uncontrolled and controlled states at $F_n = 0.40$ ($H_s = 1.00$ m).

Table 4: Uncontrolled and controlled vertical responses at $F_n = 0.40$ ($H_s = 0.88$ metres).

	Uncontrolled	Controlled ($\mathcal{H}_\infty$)	Controlled (MPC)
Pitch Motion (rms) (rad.)	0.00742	0.00672	0.00356
Bow Vertical Acceleration (rms) (m/s^2)	0.9767	0.9162	0.4401
Stern Vertical Acceleration (rms) (m/s^2)	0.4809	0.4397	0.2466
CoG Acceleration (rms) (m/s^2)	0.2985	0.3039	0.1998

of the controller is also dependent of excitation terms. That is the reason why a direct proportional relation may not set for the motion reductions at $F_n = 0.40$ and $F_n = 0.50$.

Ship accelerations, especially the vertical ones, have a great impact on the human body since they may cause motion sickness. The term motion sickness on ships is named as seasickness and it is a health problem

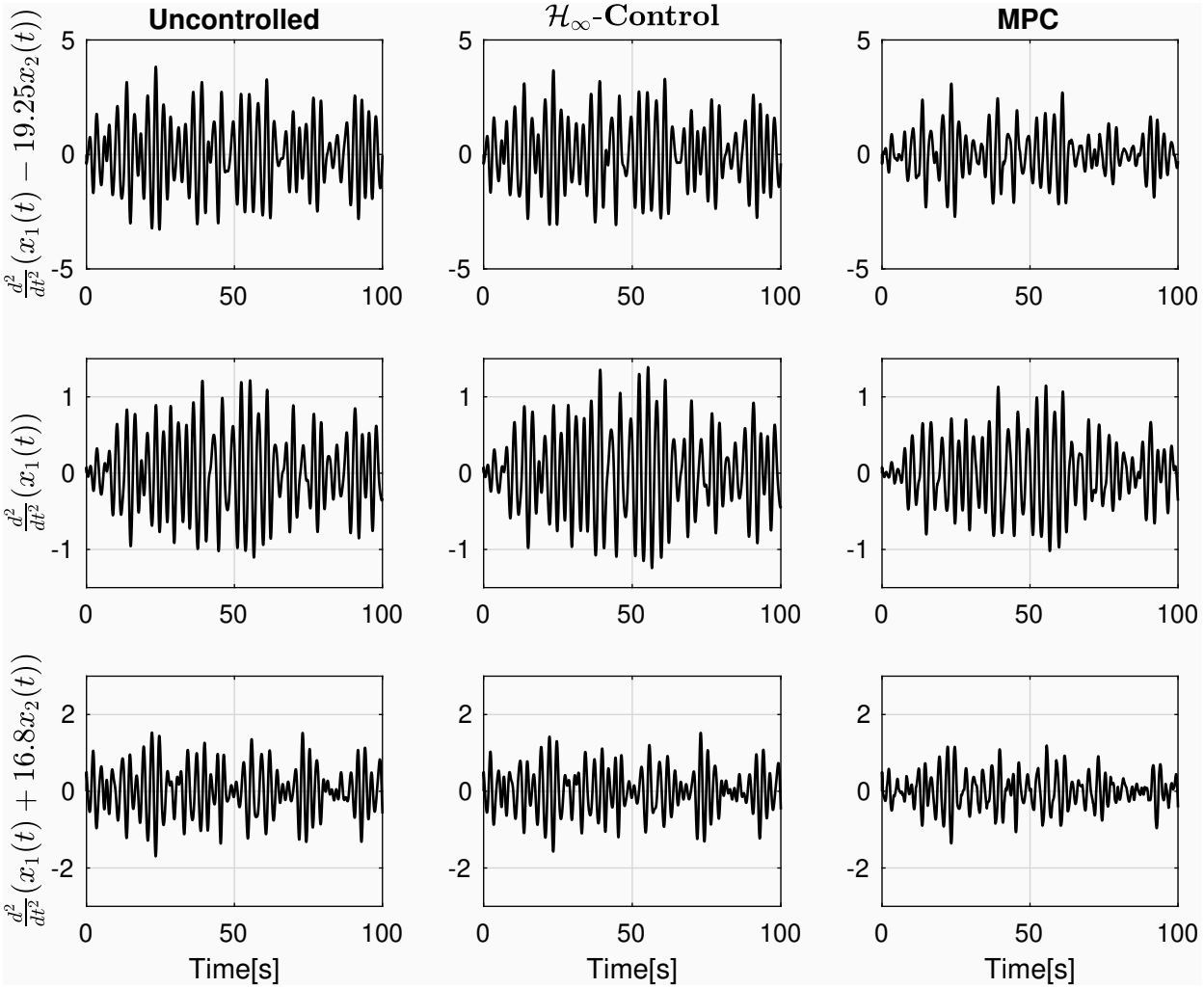

Figure 14: Time histories of uncontrolled and controlled accelerations at $F_n = 0.40$ ($H_s = 1.00$ m).

Table 5: Uncontrolled and controlled vertical responses at $F_n = 0.40$ ($H_s = 1.00$ metres).

	Uncontrolled	Controlled ($\mathcal{H}_\infty$)	Controlled (MPC)
Pitch Motion (rms) (rad.)	0.01052	0.00982	0.00708
Bow Vertical Acceleration (rms) (m/s^2)	1.4439	1.4127	0.9498
Stern Vertical Acceleration (rms) (m/s^2)	0.6079	0.5573	0.4283
CoG Acceleration (rms) (m/s^2)	0.4926	0.53293	0.4162

due to ship motions that may result in physical discomfort on the body. Seasickness might cause irregular breathing, nausea, vertigo and vomiting. The Motion Sickness Index (MSI) is commonly used for assessing the likely occurrence of the illness. As discussed in [28], MSI can be expressed as a function of the mean absolute value of vertical acceleration signal and the mean peak frequency of the vertical acceleration signal.

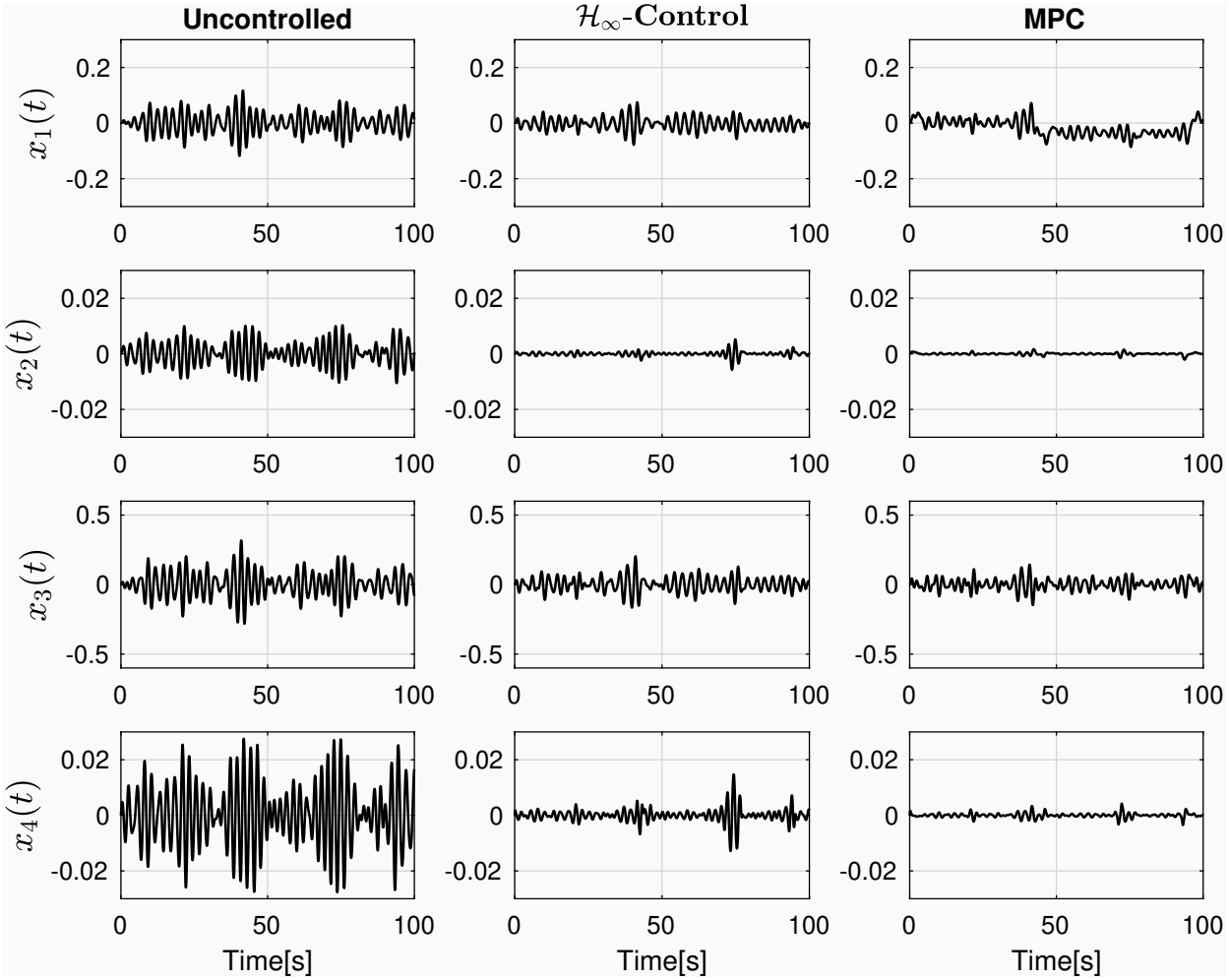

Figure 15: Time histories of uncontrolled and controlled states at $F_n = 0.50$ ($H_s = 0.70$m).

Table 6: Uncontrolled and controlled vertical responses at $F_n = 0.50$ ($H_s = 0.70$ metres).

	Uncontrolled	Controlled ($\mathcal{H}_\infty$)	Controlled (MPC)
Pitch Motion (rms) (radians)	0.00426	0.00087	0.00039
Bow Vertical Acceleration (rms) (m/s^2)	0.7885	0.2156	0.1389
Stern Vertical Acceleration (rms) (m/s^2)	0.3662	0.1552	0.0831
CoG Acceleration (rms) (m/s^2)	0.2387	0.1307	0.1051

Since we have time series of vertical acceleration data for uncontrolled and controlled cases, both values can be obtained easily and finally MSI can be calculated. Table 11 shows the MSI for uncontrolled and controlled (MPC) cases for different locations on the ship and different sea states as regards the two hours cruise ($F_n = 0.50$). Results indicate that a significant decrease in the MSI values are observed in $H_s = 0.70$

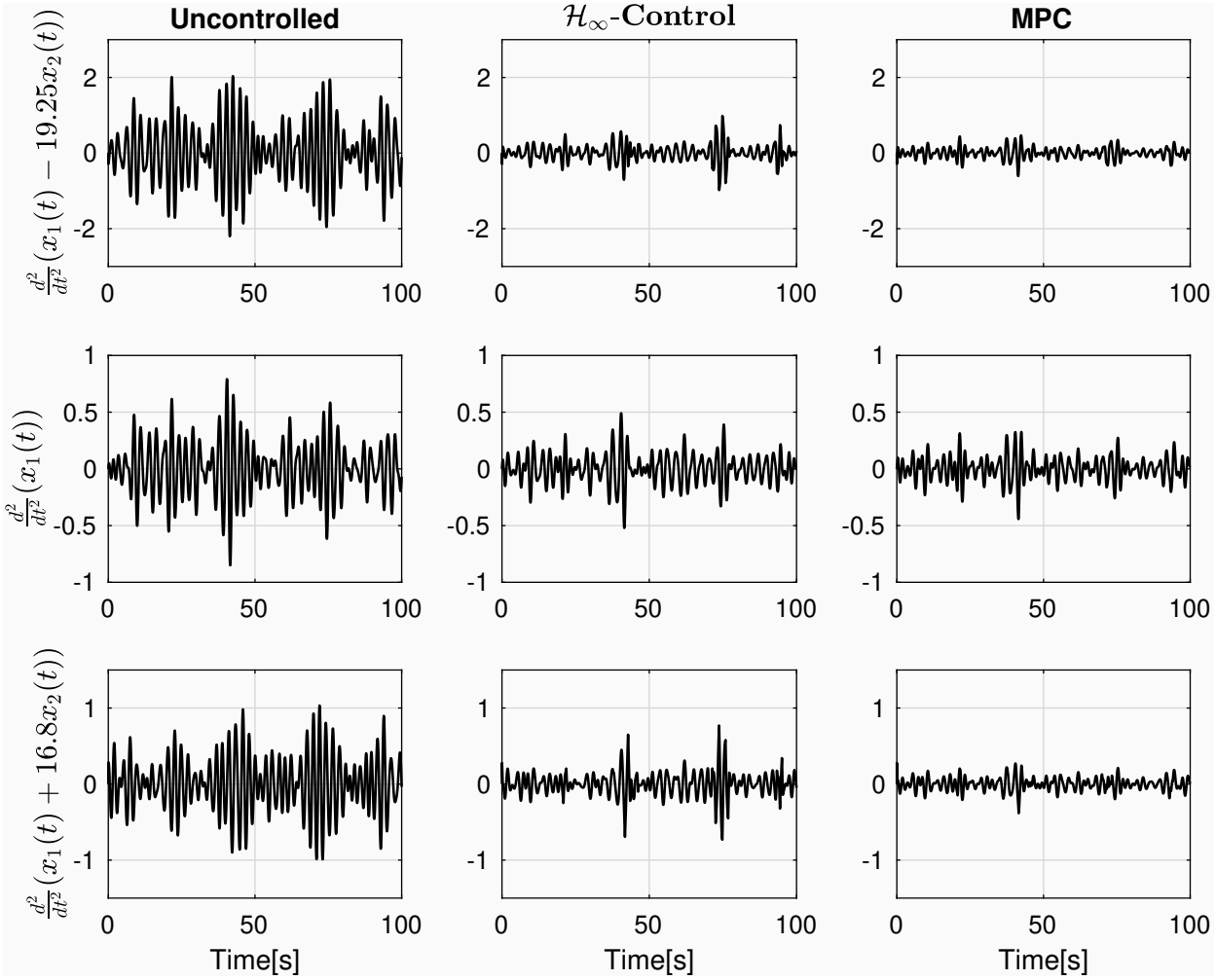

Figure 16: Time histories of uncontrolled and controlled accelerations at $F_n = 0.50$ ($H_s = 0.70$m).

Table 7: Uncontrolled and controlled vertical responses at $F_n = 0.50$ ($H_s = 0.88$ metres).

	Uncontrolled	Controlled ($\mathcal{H}_\infty$)	Controlled (MPC)
Pitch Motion (rms) (rad.)	0.00842	0.00653	0.00459
Bow Vertical Acceleration (rms) (m/s^2)	1.3835	1.1374	0.8156
Stern Vertical Acceleration (rms) (m/s^2)	0.6663	0.5698	0.3863
CoG Acceleration (rms) (m/s^2)	0.4083	0.3850	0.2987

and remarkable improvements are observed even in higher sea states.

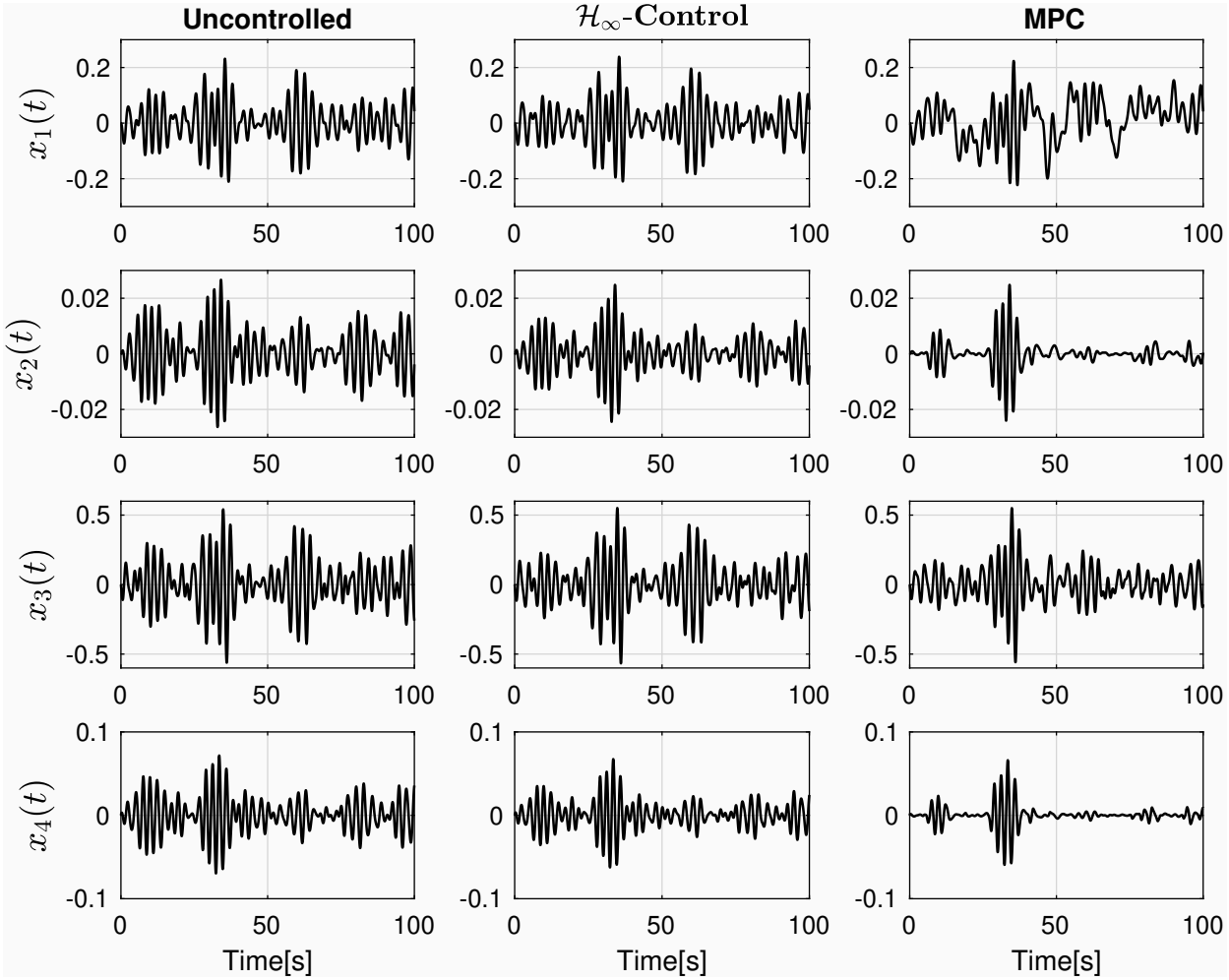

Figure 17: Time histories of uncontrolled and controlled states at $F_n = 0.50$ ($H_s = 0.88$ m).

Table 8: Uncontrolled and controlled vertical responses at $F_n = 0.50$ ($H_s = 1.00$ metres).

	Uncontrolled	Controlled ($\mathcal{H}_\infty$)	Controlled (MPC)
Pitch Motion (rms) (rad.)	0.01095	0.008554	0.00663
Bow Vertical Acceleration (rms) (m/s^2)	1.6248	1.3636	0.9689
Stern Vertical Acceleration (rms) (m/s^2)	0.8348	0.7207	0.4581
CoG Acceleration (rms) (m/s^2)	0.5045	0.5124	0.4125

6. Conclusion

In this study, it was aimed to reduce the vertical accelerations of a passenger ship which is operating at two different advance speed and in the different level magnitude of head waves. For this reason, Cummins' equation was solved with the time domain identification of fluid memory effects. Firstly, radiation terms

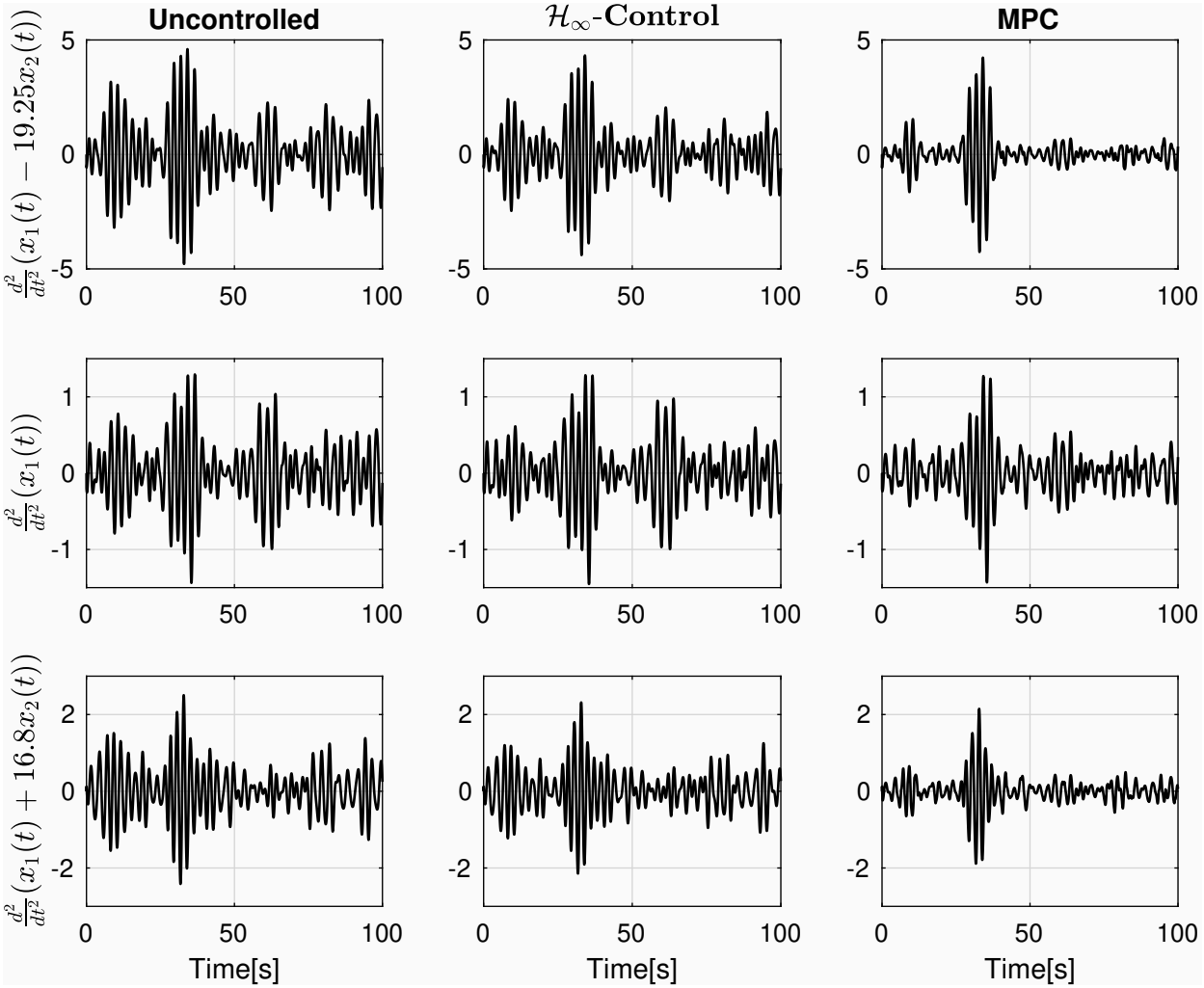

Figure 18: Time histories of uncontrolled and controlled accelerations at $F_n = 0.50 (H_s = 0.88$ m).

Table 9: Percentages improvements of accelerations at different sea states ($F_n = 0.40$) by MPC.

	% Improvement at $H_s = 0.70$	% Improvement at $H_s = 0.88$	% Improvement at $H_s = 1.00$
Pitch Motion	72.36	51.97	32.64
Bow Vertical Acceleration	75.09	54.93	34.21
Stern Vertical Acceleration	63.97	48.71	29.54
CoG Acceleration	48.56	31.22	15.49

were calculated in the frequency domain. By the aid of the information in the frequency domain, all parameters in the Cummins' equation were set for the solution in the time domain. The heave force and pitch moment acting on the ship due to irregular head waves were predicted in the time domain by the

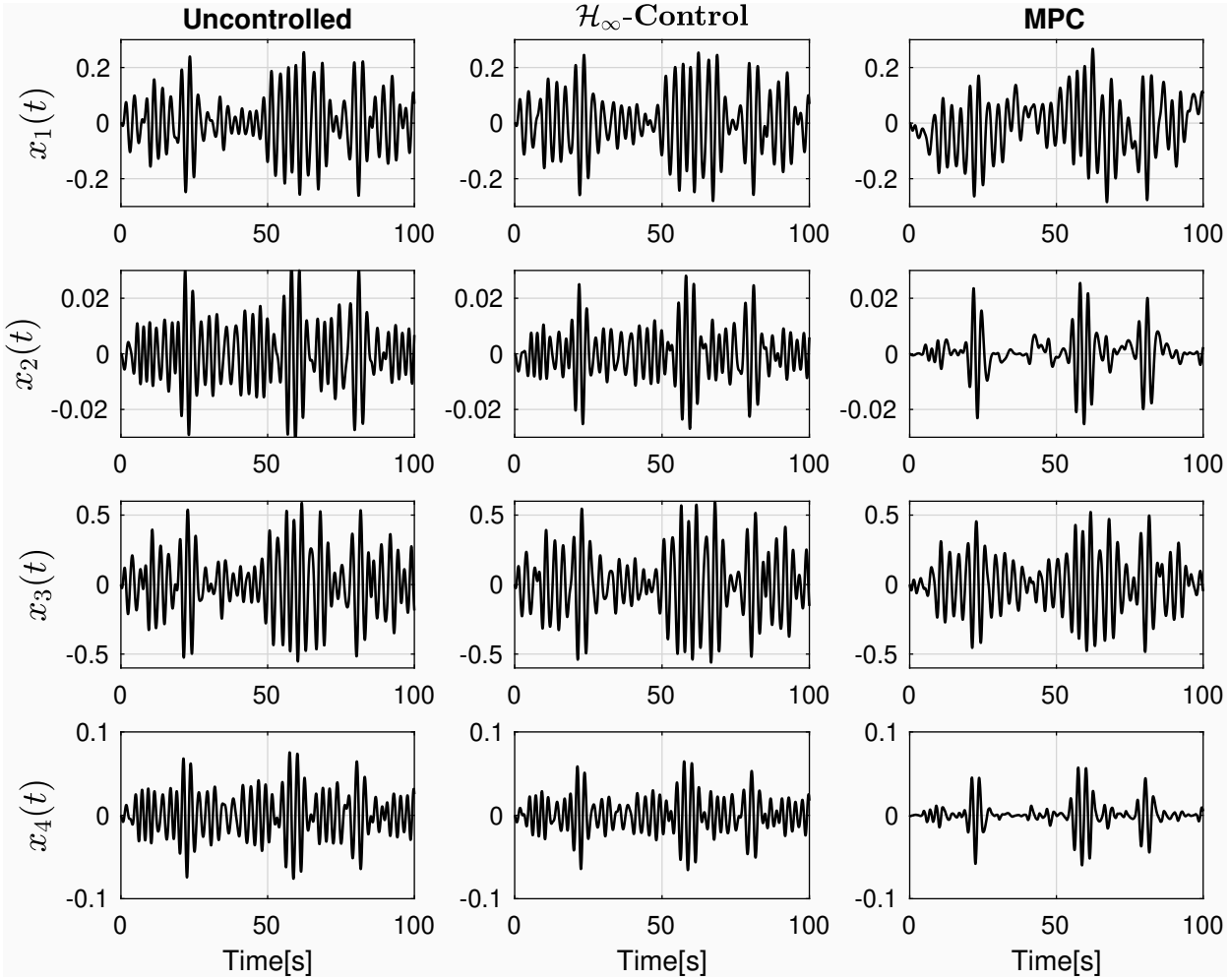

Figure 19: Time histories of uncontrolled and controlled states at $F_n = 0.50$ ($H_s = 1.00$ m).

Table 10: Percentages improvements of accelerations at different sea states ($F_n = 0.50$) by MPC.

	% Improvement at $H_s = 0.70$	% Improvement at $H_s = 0.88$	% Improvement at $H_s = 1.00$
Pitch Motion	90.67	45.47	39.42
Bow Vertical Acceleration	82.37	41.04	40.36
Stern Vertical Acceleration	77.32	42.01	45.12
CoG Acceleration	55.93	26.84	18.23

randomization process of the excitation response spectra. Then, an optimal MPC was designed to reduce the vertical accelerations. During operation of the passenger ship, all states were measured with sensors because MPC works with full state feedback procedure. The designed MPC focused on reducing pitch motion

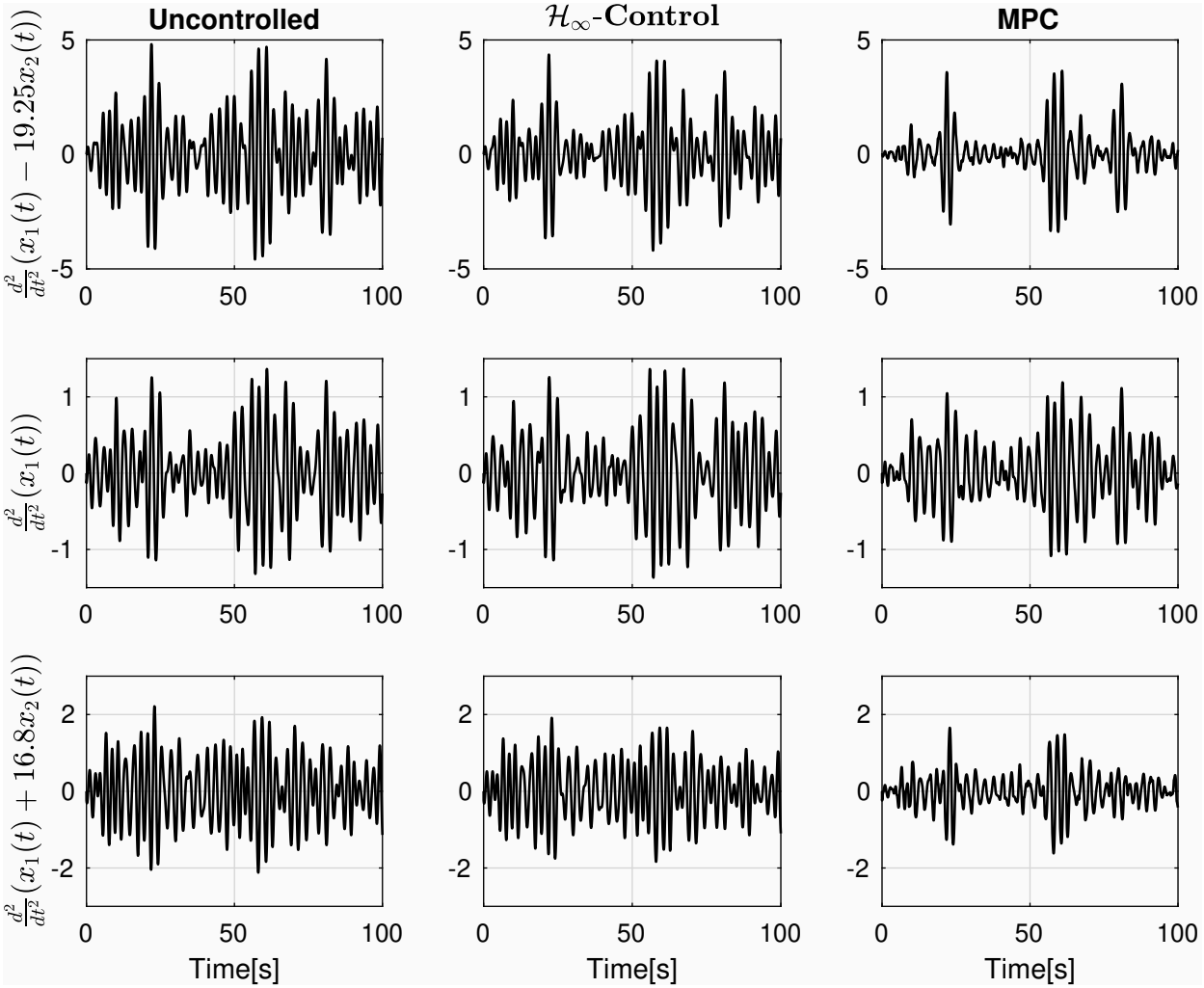

Figure 20: Time histories of uncontrolled and controlled accelerations at $F_n = 0.50$ ($H_s = 1.00$ m).

Table 11: Percentage MSI values for uncontrolled case (NC) and model predictive controlled case (C) at different significant wave heights(H_s) ($F_n = 0.50$).

	MSI $H_s = 0.70$ NC[%] - C[%]	MSI $H_s = 0.88$ NC[%] - C[%]	MSI $H_s = 1.00$ NC[%] - C[%]
Bow Vertical Acceleration	$1.32 - 0.0002$	$6.91 - 0.27$	$8.34 - 0.60$
Stern Vertical Acceleration	$0.069 - 0.0000156$	$0.98 - 0.02$	$1.91 - 0.07$
CoG Acceleration	$0.037 - 0.0002$	$0.20 - 0.03$	$0.85 - 0.37$

and velocity. The results showed that MPC results present better performance than $\mathcal{H}_\infty$ discrete time state feedback controller since MPC has advantages in a wave attenuation problem with its preview capability of excitations and handling the constraints. Thanks to the designed MPC discrete based controller, vertical

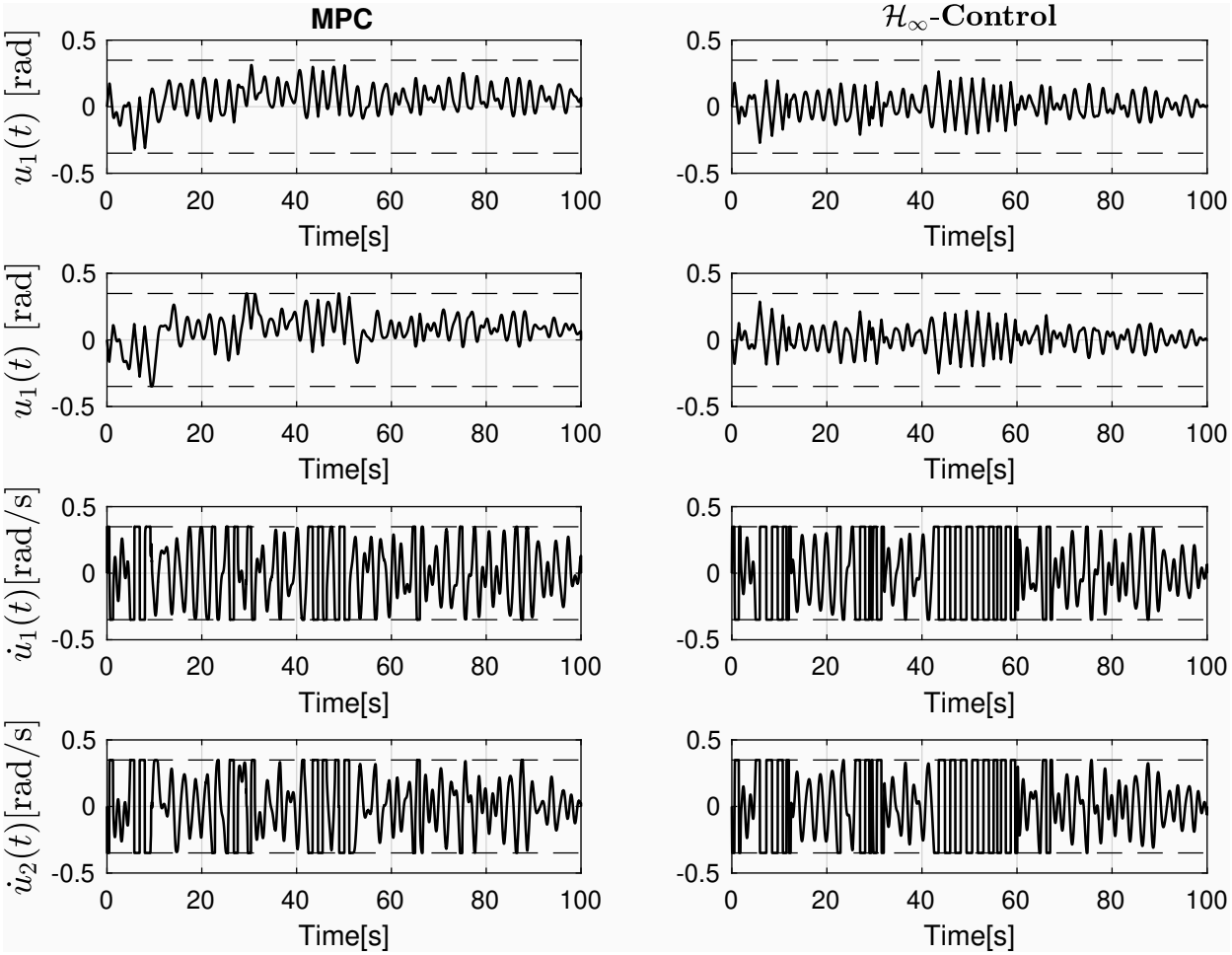

Figure 21: Time Histories of bow and stern foil angles and rates ($H_s = 0.70$ m) at $F_n = 0.40$. Here, dotted horizontal lines represent the physical bounds on the corresponding actuator signal.

accelerations in the bow, centre and stern locations of the ship were reduced by approximately 75%, 64% and 49%, respectively with a significant reduction of pitch motion in $H_s = 0.70$ metres at $F_n = 0.40$). On the other hand, vertical accelerations in the bow, centre and stern locations of the ship were reduced by approximately 82%, 77% and 56%, respectively in $H_s = 0.70$ metres at $F_n = 0.50$). As the magnitude of the sea state increases to $H_s = 0.88$ and 1 metres, the reduction rates were decreased to the level of 45% due to the excitation terms are remarkably increased for both F_n. In other words, as the foils have strict limitations on their opening angles and rotation rates, improvements in the performance of controllers were decreased. It was noted that, in contrast to pitch motion, the same motion reduction was not observed for the heave motion and midship acceleration due to the phase differences between the pitch and heave motions.

In contrast to the general belief in the community which states that active motion attenuation can only be effective on high-speed ships, the results of this study showed that MPC could still provide remarkable

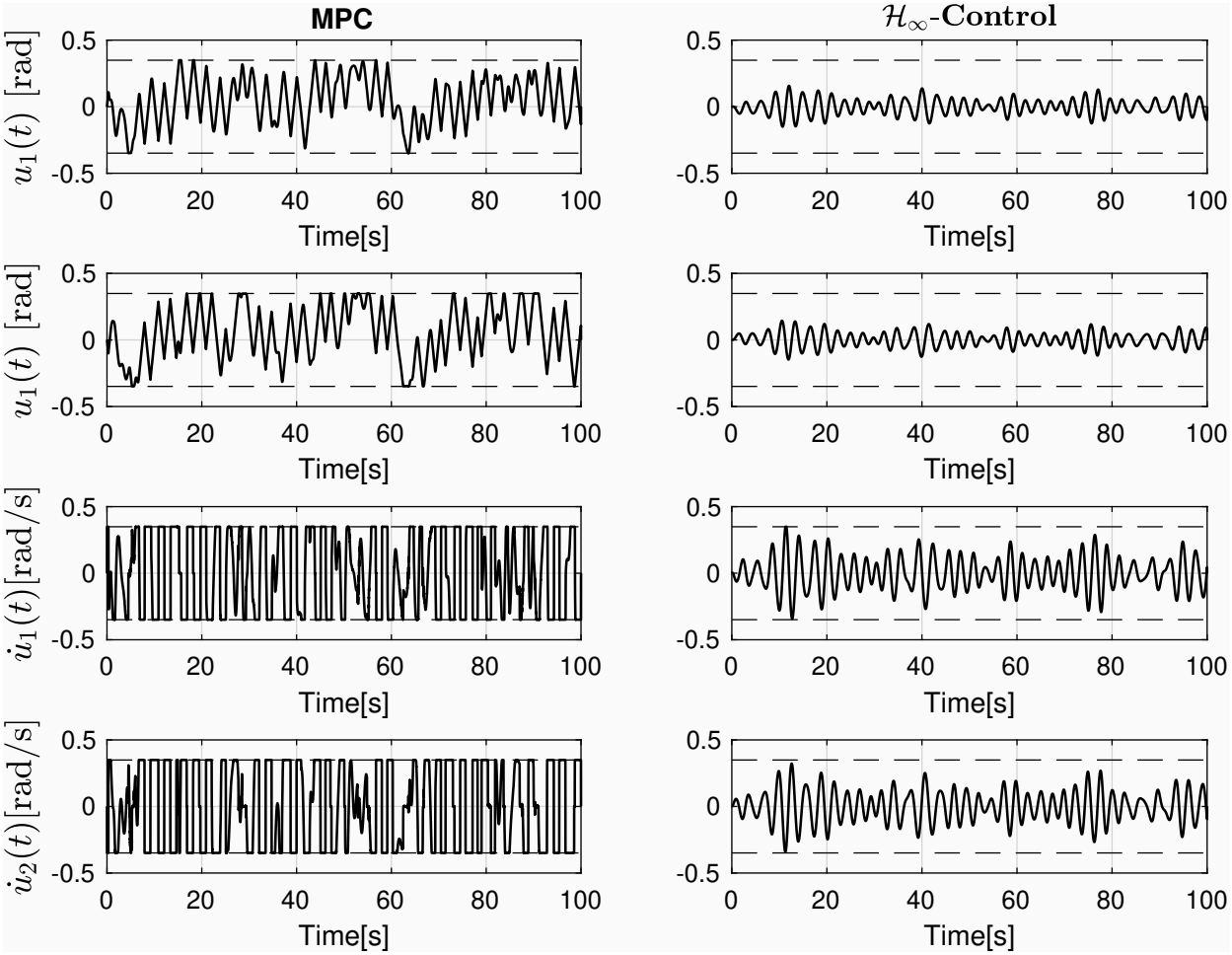

Figure 22: Time histories of bow and stern foil angles and rates ($H_s = 0.88$ m) at $F_n = 0.40$. Here, dotted horizontal lines represent the physical bounds on the corresponding actuator signal.

performance even on moderate-speed vessels having strict actuator amplitude and rate limits. The developed MPC presents favourable performance even for the displacement ship speed range *i.e* $F_n \cong 0.4 - 0.5$. As a planned future study, the estimator design will be regarded in order to avoid the obligation of measuring all states during a ship voyage. Also, the problem of controlling the vertical ship motions under varying speeds has been left as a future study since the topic falls into the scope of a linear parameter varying type MPC design.

Acknowledgements

The second author was supported by ASELSAN Graduate Scholarship for Turkish Academicians.

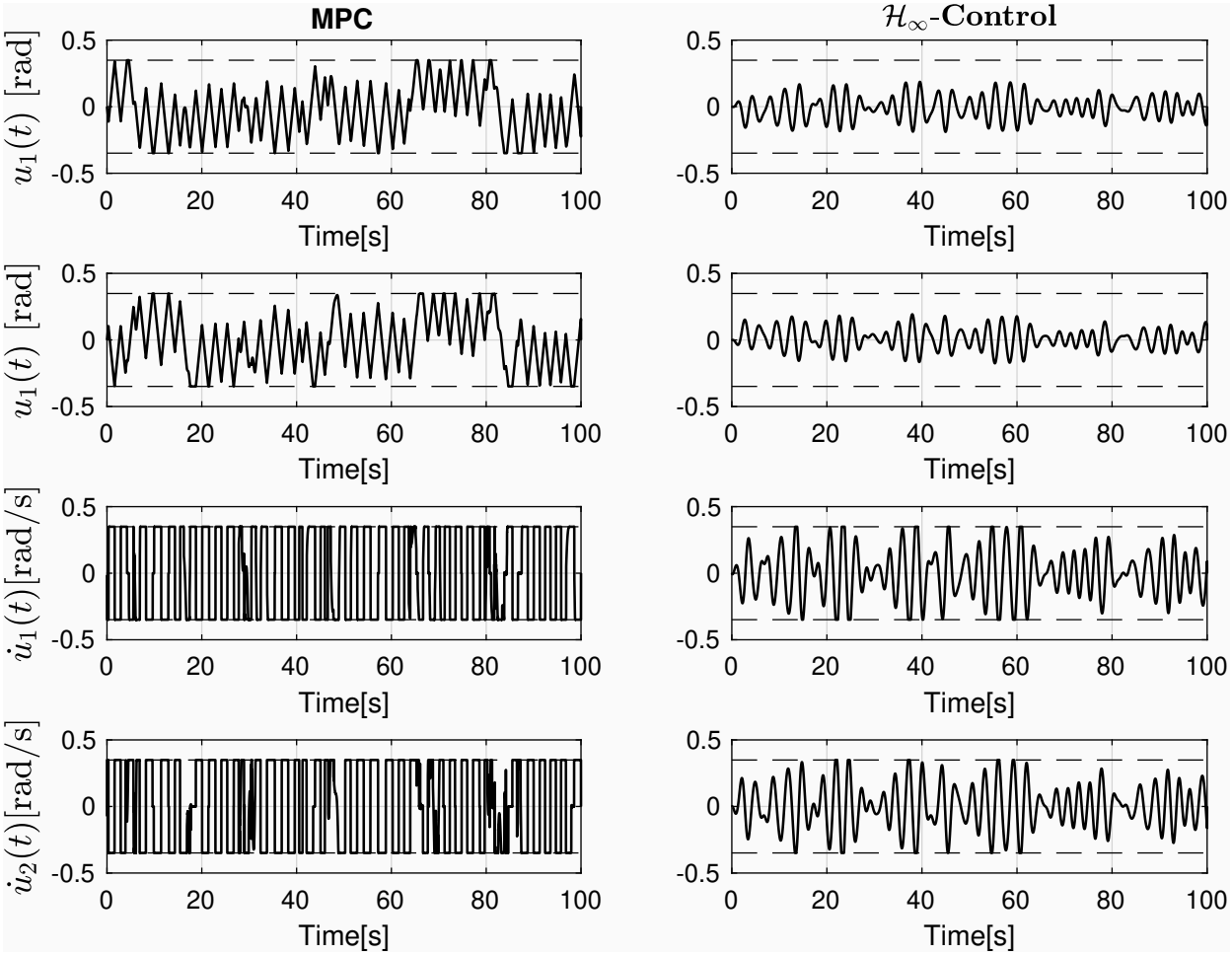

Figure 23: Time histories of bow and stern foil angles and rates ($H_s = 1.00$ m) at $F_n = 0.40$. Here, dotted horizontal lines represent the physical bounds on the corresponding actuator signal.

References

[1] J. F. O'Hanlon, M. E. McCauley, Motion sickness incidence as a function of acceleration of vertical sinusoidal motion, Aerospace Medicine 45 (1974) 366–369.

[2] E. V. Lewis, Ship speeds in irregular seas, Trans. SNAME (1955) 134–202.

[3] M. A. Abkowitz, The effect of anti-pitching fins on ship motions, Trans. SNAME (1959) 210–252.

[4] J. Avis, Use of anti-pitch hydrofoil to reduce added resistance of a yacht in waves, Marine Technology and SNAME News 28 (1991) 14–22.

[5] T. Perez, Course Keeping and Roll Stabilisation Using Rudder and Fins, Springer, 2005.

[6] L. Huang, Y. Han, W. Duan, Y. Chen, S. Ma, Numerical and experimental studies on a predictive control approach for pitch stabilization in heading waves, Ocean Engineering (2018) 388–400.

[7] S. Esteban, J. M. Giron-Sierra, B. A. Toro, J. M. De la Cruz, Development of a control-oriented model of the vertical motions of a fast ferry, Journal of Ship Research 48 (2004) 218–230.

[8] J. M. Giron-Sierra, S. Esteban, B. Andres, J. M. S. Martinez, J. Riola, Experimental study of controlled flaps and t-foil

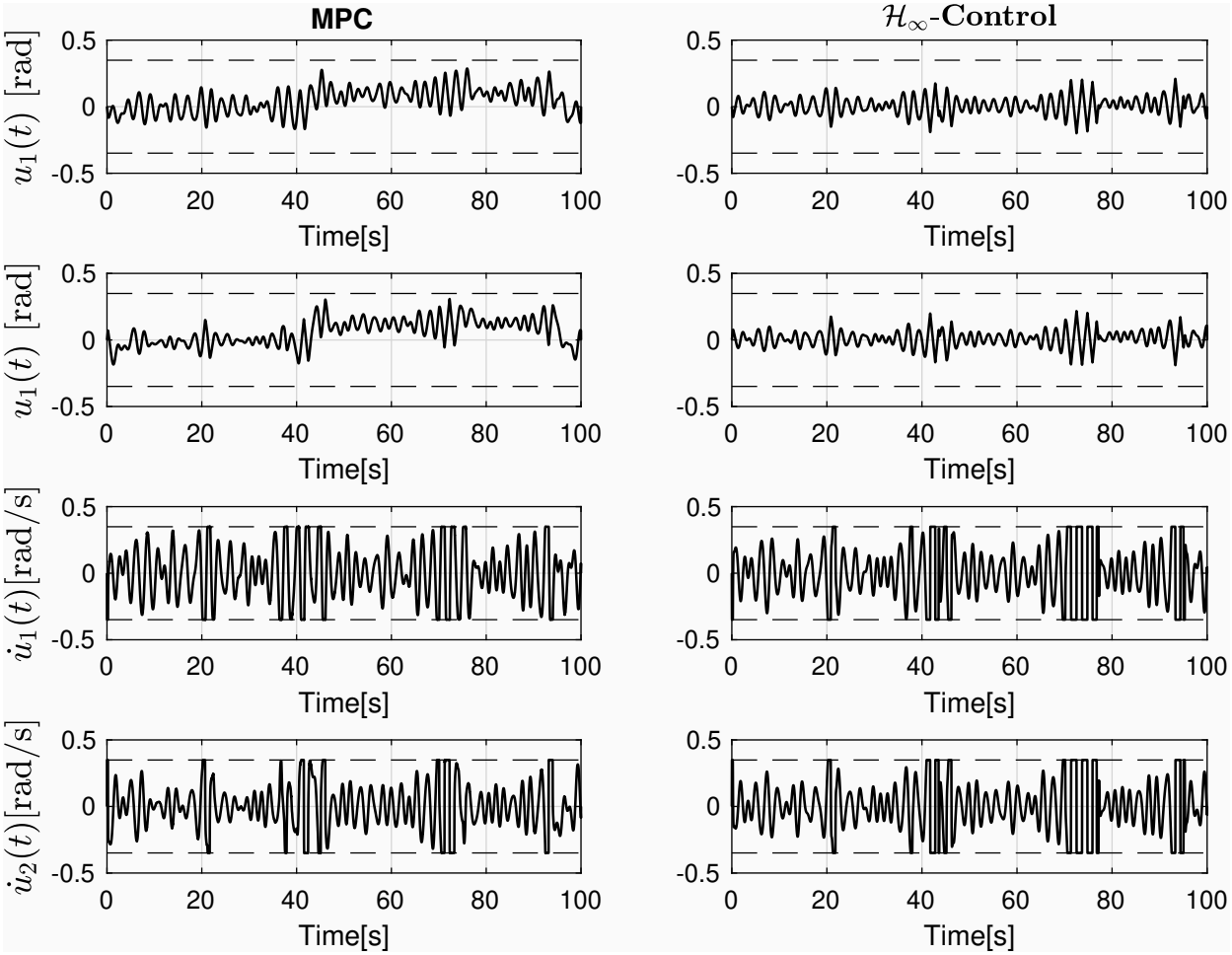

Figure 24: Time Histories of bow and stern foil angles and rates ($H_s = 0.70$ m) at $F_n = 0.50$. Here, dotted horizontal lines represent the physical bounds on the corresponding actuator signal.

for comfort improvement of a fast ferry, in: Control Application in Marine System, IFAC Conference, 2001.

[9] R. López, M. Santos, O. Polo, S. Esteban, Experimenting a fuzzy controller on a fast ferry, in: Control Applications, 2002. Proceedings of the 2002 International Conference on, Vol. 2, IEEE, 2002, pp. 1082–1087.

[10] M. Ticherfatine, Z. Quidan, Model free approach based on intelligent pd controller for vertical motion reduction in fast ferries, Turkish Journal of Electrical Engineering and Computer Sciences 6 (2018) 393–406.

[11] M. Ticherfatine, Z. Quidan, Fast ferry smoothing motion via intelligent pd controller, Journal of Marine Science And Applications 17 (2018) 273–279.

[12] S. Zhang, M. Sun, L. Liang, S. Li, H-infinity output feedback control method for the t-foil of the wave piercing catamaran, in: Intelligent Control and Automation (WCICA), 2014 11th World Congress on, IEEE, 2014, pp. 4338–4343.

[13] L. Huang, Y. Han, W. Duan, Y. Zheng, S. Ma, Ship pitch-roll stabilization by active fins using a controller based on onboard hydrodynamic prediction, Ocean Engineering (2018) 212–227.

[14] F. Cakici, H. Yazici, A. D. Alkan, Optimal control design for reducing vertical acceleration of a motor yacht form, Ocean Engineering 169 (2018) 636–650.

[15] F. Borrelli, A. Bemporad, M. Morari, Predictive control for linear and hybrid systems, Cambridge University Press, 2017.

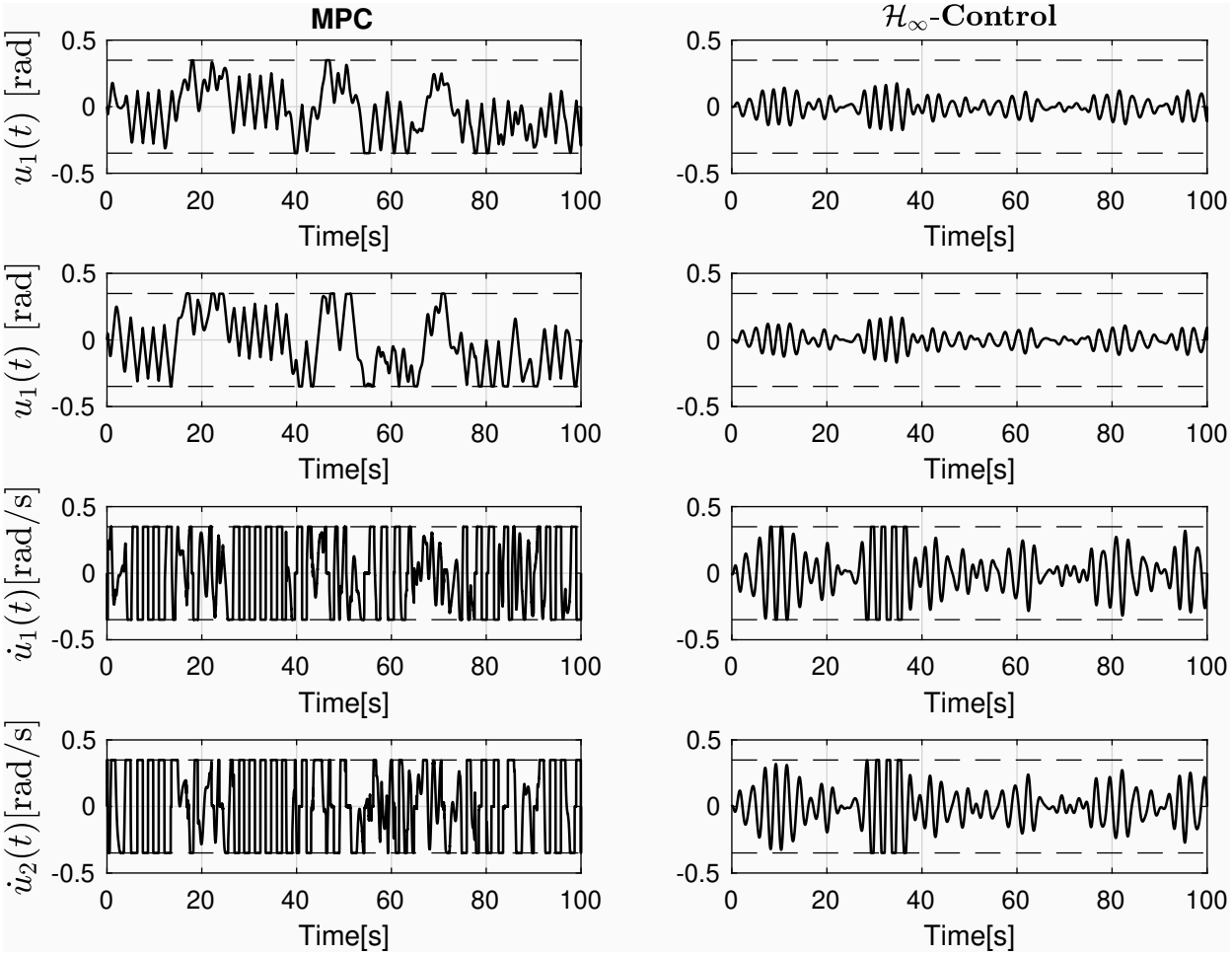

Figure 25: Time histories of bow and stern foil angles and rates ($H_s = 0.88$ m) at $F_n = 0.50$. Here, dotted horizontal lines represent the physical bounds on the corresponding actuator signal.

[16] I. Kose, F. Jabbari, Control of systems with actuator amplitude and rate constraints, Vol. 6, American Control Conference, USA, 2001, pp. 4914–4919.

[17] W. Cummins, The impulse response function and ship motions, Schiffstechnikl 9 (1962) 101–109.

[18] S. Bochner, K. Chandrasekharan, et al., Fourier transforms, Princeton University Press, 1949.

[19] M. Alves, M. Vicente, A. Sarmento, M. Gurerinel, Implementation and verification of a time domain model to simulate the dynamics of owc's, in: 9th European Wave and Tidal Energy Conference, 2011.

[20] J. F. Hauer, C. J. Demeure, L. L. Scharf, Initial results in prony analysis of power system response signals, IEEE Transactions on Power Systems 5 (1) (1990) 80–89.

[21] W. J. Pierson Jr, L. Moskowitz, A proposed spectral form for fully developed wind seas based on the similarity theory of SA Kitaigorodskii, Journal of geophysical research 69 (24) (1964) 5181–5190.

[22] M. St Denis, W. Pierson, On the motions of ships in confused seas, Trans. Soc. Nav. Archit. Mar. Eng. 61 (1953) 280–354.

[23] J. H. Kim, Y. H. Kim, Motion control of a cruise ship by using active stabilizing fins, Proc. IME M J. Eng. Marit. Environ 225 (4) (2011) 311–324.

[24] K. Hu, D. Yong, W. Hongwei, High-speed catamaran's longitudinal motion attenuation with active hydrofoils, Polish

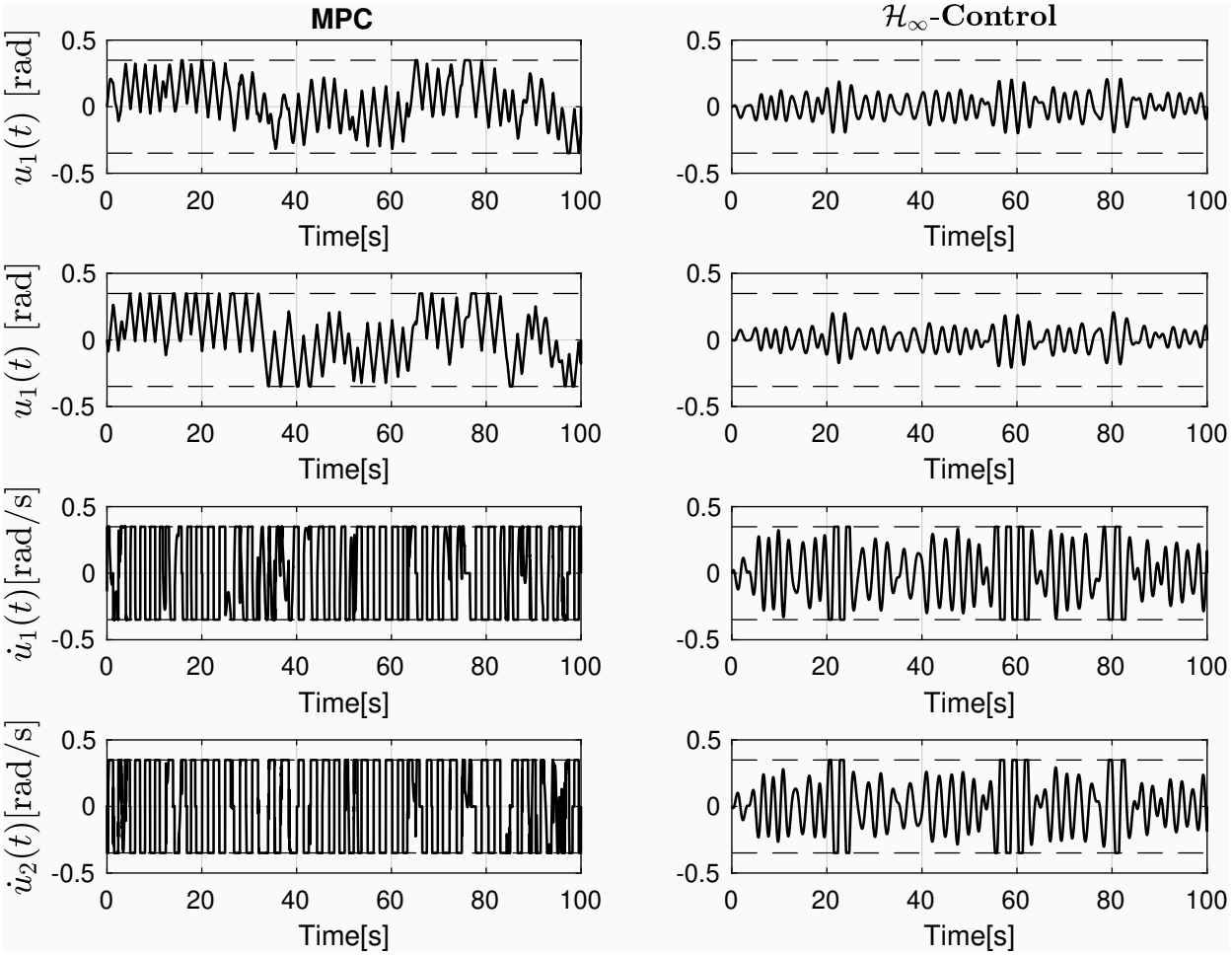

Figure 26: Time histories of bow and stern foil angles and rates (H_s = 1.00 m) F_n = 0.50. Here, dotted horizontal lines represent the physical bounds on the corresponding actuator signal.

Maritime Research 25 (2018) 56–61.

[25] M. Sadeghi Reineh, S. S. Kia, F. Jabbari, New anti-windup structure for magnitude and rate limited inputs and peak-bounded disturbances, Automatica 97 (2018-11) 301,305.

[26] S. Boyd, L. El Ghaoui, E. Feron, V. Balakrishnan, Linear Matrix Inequalities in System and Control Theory, SIAM studies in applied mathematics: 15, 1994.

[27] J. Löfberg, Yalmip : A toolbox for modeling and optimization in matlab, in: In Proceedings of the CACSD Conference, Taipei, Taiwan, 2004.

[28] A. Lloyd, Seakeeping: Ship Behaviour in Rough Weather, Ellis Horwood series in marine technology, A.R.J.M. Lloyd, 1998.

LaTeX Source for the revised paper

Click here to download LaTeX Source Files: revised paper_Ocean Engineering.rar